DUAL COMB SPECTROSCOPY WITH MISMATCHED COMBS

by

TODD ELIASON

(Under the Direction of Melanie Reber)

ABSTRACT

Dual comb spectroscopy is a high resolution spectroscopic technique. It requires two frequency combs which are lasers comprised of equally spaced narrow linewidth lasers. Dual comb spectroscopy can resolve the intensity of individual comb teeth, which is independent of the wavelength of the frequency combs used. Often two matched frequency combs are used because of the mutual coherence and stability required to perform dual comb spectroscopy. This work seeks to design and build an dual comb spectrometer with two combs in the same spectral region generated by different methods. The first comb is electro-optic frequency comb that has a highly stable mode spacing with a larger bandwidth than other examples of electro-optic combs. The second frequency comb is a Yb fiber oscillator matched to lasers used in other experiments in the group. To validate this method, these two frequency combs are used to characterize ammonia in a gas cell. These initial steps lay the ground work for using dual comb spectroscopy/detection in transient absorption and 2D spectroscopy experiments.

INDEX WORDS: [Frequency Combs, Electro-optic Comb, Dual Comb]

DUAL COMB SPECTROSCOPY WITH MISMATCHED COMBS

by

TODD ELIASON

B.S., University of North Georgia, 2019

A Dissertation Submitted to the Graduate Faculty of the University of Georgia in Partial Fulfillment of the Requirements for the Degree.

Doctor of of Philosophy

ATHENS, GEORGIA

©2025 Todd Eliason All Rights Reserved

DUAL COMB SPECTROSCOPY WITH MISMATCHED COMBS

by

TODD ELIASON

Major Professor: Melanie Reber

Committee: Gary Douberly

Mabel Fok

Electronic Version Approved:

Ron Walcott Dean of the Graduate School The University of Georgia May 2025

DEDICATION

For my Bebo.

ACKNOWLEDGMENTS

Thank you to everyone who supported me through this degree. I want to offer thanks to Dr. Melanie Reber for all of her help and always fielding my questions. I want to thank Mabel Fok for allowing me to use her lab because of the frequent floods in the chemistry building. I want to thank all of the members of the group, that were always available to have technical discussion and support when experiments were going awry. I would like to acknowledge the support and patience of my wife, because without her support I would not have been able to complete this work. I want to also thank all of my family for their support as well, it truly takes a village to make anything possible.

Contents

Acknowledgments				
List of Figures				
I	Intr	oduction	1	
	I.I	Frequency Combs	I	
	1.2	Dual Comb Spectroscopy	3	
	1.3	TA and 2D Experiments	4	
	I.4	Berry Phase	5	
2	Con	structing Electro-Optic Frequency Comb	6	
	2. I	Electro-Optic Comb Architecture	8	
	2.2	Electro-Optic Comb Performance	12	
	2.3	Sideband Strength with Harmonics	16	
3	Con	struction of a Dual Comb Spectrometer	19	
	3. I	Constructing Yb Oscillator	19	
	3.2	Dual Comb Spectrometer	23	
	3.3	Data Collection	27	
4	Amr	nonia Spectroscopy	30	
	4. I	Nd:YAG Output Frequency Tuning	30	
	4.2	Lineshape and Broadening	31	
	4.3	Dual Comb Spectra of Ammonia	33	
5	Sum	mary and Future steps.	35	
A	pend	lices	37	
A			37	
	А.1	LabVIEW Programs	40	
	A.2	MATLAB Programs	43	

79

LIST OF FIGURES

1.1	The top half is the frequency domain and the bottom is the time domain picture. The red curve is the carrier or the electric	
	field of the pulse while the black curve is the envelope function.	2
I.2	The top half is optical frequencies. The bottom half is the	
	frequency domain picture of the dual comb signal	3
2.I	EO-comb Architecture and electronic block diagram, full de-	
	tails in text. PS is a phase shifter, Phase Det. is the phase detec-	
	tor or phase comparator, VCO is a voltage controlled oscillator,	
	and 1/N is a frequency divider[13]	8
2.2	Detection Scheme. 70:30 and 50:50 are beam splitters of the	
	same ratio. PBS is a polarizing beam splitter. BB is a beam	
	block that is placed during Fabry-Perot spectra collection. BD	
	is a beam dump. FC are fiber couplers. FP is the Fabry-Perot	
	Cavity. Det A. collects the Heterodyne measurement data.	
	Det. B. collects the Fabry-Perot Spectra[13]	IC
2.3	a) RF Spectra of the 11-12.5 GHz PLL at 11.44 GHz b) RF Spec-	
	tra of the 1-2 GHz PLL at 1.04 GHz c) RF Spectra of the 75-150	
	MHz PLL at 80 MHz d) Phase noise of the RF sources. The	
	11.44 GHz source was divided by 8 to collect this data[13]	11
2.4	RF Spectra of the Nd:YAG seed laser with only the 80 MHz	
	EOM Modulation on beat with the 260 MHz AOM modu-	
	lated laser. Racetracks denote the positive and negative modu-	
	lations referenced from the seed laser. The unmodulated seed	
	laser is the 0^{th} mode. The light blue section of spectra is multi-	
	plied by 4, the purple section multiplied by 8, and the 1/f noise	
	removed for clarity[13]	13

2.5	RF Spectra a) Selection of the RF Spectrum from 490-1000	
	MHz, The EO-comb signal is shifted up by 0.5 mW. The	
	racetracks denote the comb tooth number from the seed laser	
	for the positive and negative sides of the EO-comb. b) Phase	
	noise of the instrument (black line), AOM modulated seed	
	laser (blue circle), single modulation at 1.04 GHz (pink circle)	
	and 80 MHz (purple square), and the full comb (gray square)[13].	14
2.6	Fabry-Perot Spectra a) seed laser modulated at 11.44 GHz b)	
	seed laser modulated by 1.04 GHz c) The spectrum collected	
	of the full EO-comb, averaged 3 times[13]	15
2.7	Fabry-Perot Spectra a) Trace of 11.44 and 1.04 GHz modula-	
,	tion. The harmonic numbers are measured from the seed laser	
	which is set to o GHz. b) Trace of the 11.44 and 1.2 GHz modu-	
	lation. The black racetrack is counting 1.2 GHz modes starting	
	at the seed laser. The blue racetrack is counting modes gener-	
	ated from the -11.44 GHz mode. The peak width is limited by	
	the Fabry-Perot cavity and is not a measure of the comb tooth	
	width[13]	16
2.8	RIN collected of the background, YAG seed laser, and the EO-	
	comb. For frequencies higher than 1 kHz, a low-noise ampli-	
	fier (LNA) was used after the detector to increase the signal	
	above the detector noise floor. The RIN is dominated by the	
	Nd:YAG seed laser[13]	17
3.1	This is a diagram of the laser cavity of the Yb fiber oscillator.	
	WDM is a wave division multiplexer. $\lambda/2$ and $\lambda/4$ are half	
	and quarter waveplates respectively. PBS is a polarizing beam	
	splitter. G1 and G2 are 600 lines/mm gratings. RF is a retrore-	
	flector. M1 and M2 are protected silver mirrors	20
3.2	This is a spectrum of the oscillator. This lock was chosen due	
	to the high intensity around 1064 nm	21
3.3	The solid blue line is the calculated change in path length. The	
	orange circles denote experimental changes in path length of the oscillator.	
2 4		22
3.4	The different colors denote data taken on different days. The	
	x axis is the frequency of the II.25 V_{pp} triangle wave. The Y axis	. .
	is the f_0 beat note range in Hz. \dots	23

3.5	The dotted lines denote fiber optics. The solid lines are free-space optics. The dotted green lines denote RF connections. The oscillator and EO-comb are simplified for clarity. They are combined in free space and fiber coupled. The fiber coupled light is incident upon a detector that collects the sample and reference arms, and both signals are sent to the data acquisition board. The f_0 beat note is collected in tandem with the dual
	comb data
3.6	Repetition rate lock
3.7	f_0 Locking scheme. After the detector multiple RF filters are used however just a band-pass filter is shown before the offset
	controller
3.8	The blue curve is the Fourier transform of the time domain data. The black circle denotes the beat note of the fundamental Nd:YAG. The orange/black circles denote the data points
	that would be collected for constructing the spectrum 28
	that would be concered for constructing the spectrum
4.I	The black curve is a modeled NH_3 spectrum from Hitran. The
	red curve is the modeled bandwidth of the EO-comb 30
4.2	The left graphs is a selection of the modeled NH ₃ spectrum.
	The right graph is the output frequency in THz of the Nd:YAG
	with crystal temperature. The color coded stars correspond to
	the two most intense transitions within the frequency tuning
	range
4.3	This figure depicts a convolution of the Doppler and pressure
	broadening line-shapes
4.4	The left graph contains the peak with a cell pressure of 248
	Torr. The right graph contains the peaks with cell pressures of
	52.1 and 150 Torr. These data sets are not on the same graph
	because the Nd:YAG crystal was at different temperatures be-
	tween these spectra, therefore it may not be the same ammonia
	transition
4.5	a) is the Voigt modeling of the ammonia spectrum at 150 Torr.
	b) Voigt modeling of the ammonia spectrum at 52.1 Torr 34
А.1	Circuit Diagram of the PLL Box. The ports that are used for
	each PLL evaluation board are labeled
A.2	Labeled Picture of the PLL Box
A.3	Circuit diagram of the Power distribution box

A.4	This is the front panel for the RF spectra auto-collection pro-	
	gram	40
A.5	This is the first part of the block diagram for the RF spectra	
	auto-collection program	41
A.6	This is the second part of the block diagram for the RF spectra	
	auto-collection program	42

CHAPTER 1

Introduction

Spectroscopy is the study of the interactions of light and matter. This covers many different interactions and processes and its applications are near endless. High resolution spectroscopy is outlined in this dissertation, which probes fundamental excitations and transitions. The structure of this dissertation is as follows Chapter 2 explores the construction of an Electro-optic frequency comb. Chapter 3 covers the construction of a Yb fiber oscillator and dual comb spectrometer (a high resolution technique). Chapter 4 explores the gas phase spectroscopy of ammonia.

1.1 Frequency Combs

Frequency combs were first developed for frequency metrology, as they can measure optical frequencies in the RF domain using RF electronics[11, 10]. Aptly named, comb lasers consist of equally-spaced, narrow-linewidth, laser lines forming the comb structure in the frequency domain[47]. Frequency comb lasers have found use in precision measurement from metrology to high-resolution spectroscopy, including absorption spectroscopy, photoacoustic spectroscopy, and others [35, 6, 36, 9, 39, 50].

There are two main parameters that define a frequency comb. The repetition rate (f_{rep}) and the f_0 . The repetition rate is the spacing of the frequency modes that comprise the comb. f_0 is the offset of the first frequency mode (see Fig 1.1). Combs also are generally pulsed lasers with pulsed separated by the period of the repetition rate, hence the name. There is also a defined phase slip between the carrier and envelope ($\Delta \phi$), this carrier envelope offset (CEO) has to be defined for a mode locked comb. Often f_{ceo} is used in place of f_0 however the CEO is not equal to f_0 but is proportional. Therefore, these terms should not be interchanged and does not clarify the physical picture.

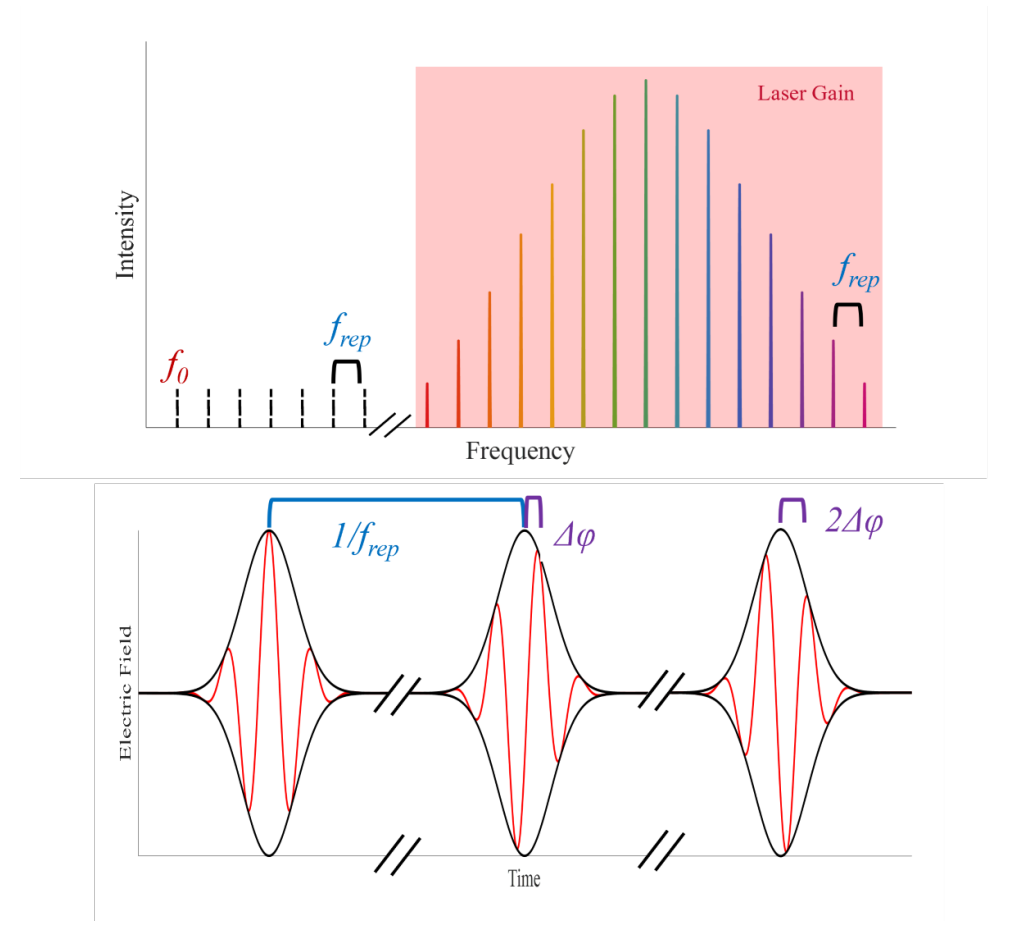


Figure 1.1: The top half is the frequency domain and the bottom is the time domain picture. The red curve is the carrier or the electric field of the pulse while the black curve is the envelope function.

The most common way to generate a frequency comb laser is by using a pulsed, mode-locked laser and stabilizing the carrier-envelope phase. Mode-locked lasers require significant ultrafast laser expertise and a controlled laboratory setting to operate [50]. There are many different methods to mode lock a laser and many PhD's worth of work to explore them all. The important thing to note is that a mode locked laser is a frequency comb, i.e. the repetition rate and CEO are stabilized. Although free-running frequency combs are combs where those parameters are not actively stabilized.

1.1.1 Electro-Optic Combs

Electro-optic combs or EO-combs are a kind of frequency comb that uses RF signals and nonlinear optical crystals to turn a CW seed laser into a frequency comb. The stability of available RF sources creates a comb with a incredibly stable repetition rate that is insensitive to environmental conditions. EO-combs offer advantages in arbitrary waveform generation, ranging, optical communications, astronomical spectrum correction, and spectrum detection, due to their highly stability and reproducibility compared to mode-locked lasers [50].

EO-combs demonstrated in literature will be discussed in depth in Chapter 2, however I will attempt to give a brief introduction here. All EO-combs consist of 3 main components: A seed laser, a RF source, and some arrangement of EOMs. There are many permutations of this simple architecture and each methods has its own advantages and disadvantages. However EO-combs allow for tailoring the laser source to the specific applications. The trade-off for EO-comb generation is a low repetition rate or higher optical bandwidth.

1.2 Dual Comb Spectroscopy

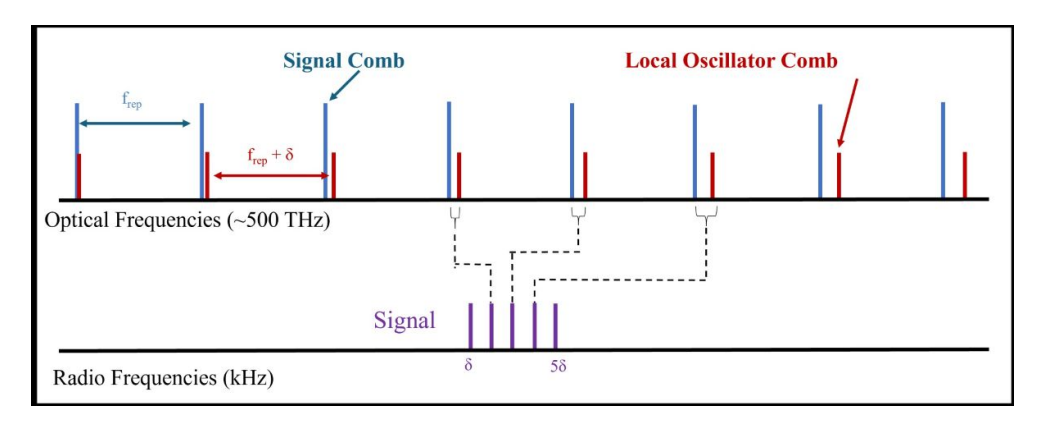


Figure 1.2: The top half is optical frequencies. The bottom half is the frequency domain picture of the dual comb signal.

Dual comb spectroscopy or simply dual comb is a high resolution technique, which requires two frequency combs. The two combs used are a signal comb that interacts with the sample and a local oscillator comb with a slightly different repetition rate. Each signal comb tooth heterodynes with a local oscillator comb tooth creating a beat note at a lower frequency. The beat notes of these comb tooth pairs are spaced by the difference in the repetition rates (see Fig 1.2). The time domain beat signal is called an interferograms and can be Fourier

transformed to resolve the beat intensities. It is important to note that the bandwidth of dual comb is limited by the number of comb teeth that can be resolved before the beat note becomes greater that the repetition rates. Dual comb can resolve the intensity of each comb tooth, which means that the resolution is limited by the comb tooth linewidth. This linewidth is typically in the kHz, however lower linewidth combs have been used for dual comb [6]. The dual comb experiment will be further explored in chapter 3, with a further discussion of the literature examples of dual comb spectroscopy.

1.2.1 High Resolution Spectroscopy

I have said that dual comb is a high resolution technique however this does not justify why high resolution spectroscopy is of interest. High resolution spectroscopy generally has frequency resolution of less than one wavenumber which is roughly 30 GHz. This high resolution is needed to distinguish between closelying spectral transitions. The simplest example is rovibrational transitions that can be observed in the mid-IR. Ammonia (NH₃) rotational transitions are separated by roughly 9 cm $^{-1}$ [12]. However different isotopes of ammonia will have slightly different rotational constants, which requires higher resolution. Rotational transition spacing will decrease with increasing molecular weight, which means higher resolution is needed to resolve the rovibrational transitions for heavier molecules. The second example I will discuss is hyperfine splitting. This splitting happens due to the nuclear spin of an atom, These splittings are typically separated by less that one wavenumber [2]. While typically observed in atomic spectroscopy, hyperfine splitting can be observed in all types of spectroscopy. High resolution spectroscopy offers the tools to probe fundamental processes of atoms and molecules.

1.3 TA and 2D Experiments

There are two other experiments in the Reber lab. These experiments are both time resolved unlike the spectroscopy contained in this work. The goal is to use dual comb spectroscopy to give ultrafast time resolved experiments high frequency resolution. The first experiment is cavity enhanced transient absorption, while this experiment is very sensitive and has 100 fs of time resolution. However, it has limited frequency resolution. To give this experiment comb tooth resolved spectra, dual comb spectroscopy will be used; to achieve this, the probe comb will be heterodyned with a local oscillator comb. The second experiment is 2D IR spectroscopy which used 3 laser pulses, two pump and

I probe to observe coupling of molecular transitions. Similar to the transient absorption experiment, the probe pulse just needs to be heterodyned with a local oscillator comb to collect high resolution spectra.

1.4 Berry Phase

Berry phase or geometric phase is a phase shift that is proposed as a wavefunction propagates around a conical intersection, in a closed loop. First, lets define a conical intersection: this process is the non-adiabatic crossing from a higher energy state to a lower energy state. If the states are adiabatic the crossing and energy transfer is forbidden. For a conical intersection to exist the states need to be near degenerate along an internal coordinate. The relaxation observed is incredibly fast and happens on ultra-fast timescales. Which is why transient absorption is needed to observe conical intersections, the pump pulse promotes a population into the higher energy stand and the probe pulse tracks the populations as a function of time. This work has been focused on high resolution spectroscopy, and if these states are short-lived the lifetime broadening will render high resolution measurements useless. However, if you probe longer lived states in the lower energy manifold, you will be able to distinguish what state the system relaxes to.

There has been recent work by Valahu et. al. showing destructive interference when a trapped ion travels around a constructed conical intersection. They were able to show destructive interference on the opposite side of the conical intersection when they propagated the nuclear wave-packet [40]. The phase collected by the wavefunction as it travels through the conical intersection should impart a phase upon the rotational states, in the higher energy vibration. This phase should interfere and change the intensities of the rotational states. This requires high resolution spectroscopy. If this hunch is correct a low resolution method would not be able to observe the phase/intensity change of these systems. This is the goal for a high resolution transient absorption dual comb spectrometer.

CHAPTER 2

CONSTRUCTING ELECTRO-OPTIC FREQUENCY COMB

EO-combs can be generated by placing EOMs either inside the laser cavity or external to the laser cavity. The first kind of EO-comb was intracavity EO-combs. One of the first examples is from Bell Laboratories in 1963, which used a single modulator in a Fabry-Perot cavity [16]. Cavity based EO-combs typically have GHz repetition rates [21, 43, 45, 25]. Some intracavity EO-combs utilize micro-resonators on chips to either create or amplify the modulation [17, 27, 42].

Alternatively, the EOM can be external to the laser cavity, used in this work, and has the advantage of separating out the laser gain dynamics from the comb generation. Extracavity EO-combs consist of one or more EOMs in series or in parallel after the CW laser output. Some EO-combs consist of one EOM modulated with a single sine wave at GHz frequencies [1, 48, 33, 32]. These single EO-combs have limited bandwidth due to number of modes than can be generated from a single EOM without exceeding the RF damage threshold. A GHz repetition rate is often used to maximize the optical bandwidth of these EO-combs, and consequently most are made with waveguide-type EOMs. Other examples of EO-combs use multiple EOMs in series, a cascaded architecture, modulated at a single frequency. Modulators in series generates broader comb because successive modulations act on the comb teeth generated previously, resulting in an overall larger bandwidth. Cascaded EO-combs often have intensity modulators along with phase modulators, driven at the same RF frequency (>10 GHz typically) [49, 24, 38, 22, 5, 26].

EO-combs are also generated by driving the EOM with complex waveforms. Chirped RF generation is a method where a swept sine wave is sent to an single EOM. While the repetition rate can be as low as kilohertz, these combs are limited to a few gigahertz in bandwidth[31, 30]. The current limitations of these architectures lie in the highest frequency of the function generator and the maximum RF power of the EOM. Chirped sine waves can also be used in series and in a cavity to generate combs[25]. Another method of modulating is called pseudo-random modulation, where a modified square wave drives the EOM creating a comb, albeit with similar limitations of chirped RF generation[41, 19, 18].

In this chapter we demonstrate a comb design that will combine the large bandwidth of single frequency RF modulation with smaller comb tooth spacing to create a comb without the limitations of the single frequency modulation combs and the complex waveform modulation combs. By diving EOMs in series with sequentially lower harmonic frequencies, we take advantage of the bandwidth of the higher repetition rate, while filling in the comb with the smaller repetition rate. There are a few examples in the literature of EOM-based combs using multiple EOMs driven at different frequencies. An early example involved an EOM in a Fabry-Perot cavity, which was driven with a higher harmonic of the Fabry-Perot modes [37]. There have also been EO-combs which contain two micro-resonators in series, first modulated at a higher frequency then modulated at a lower frequency harmonic [4, 15]. These examples are all cavity-based modulations and not purely EOM-based. There are other configurations of multiple EOMs driven at different frequencies used to make a tailored optical frequency output. Some have the higher frequency EOM first[29, 28, 44] and some with the lower frequency EOM first[20, 23], which provides necessary background for combining multiple EOMs.

Since the EO-comb in this work is driven by multiple frequencies, phase-locked loops (PLL) are used to frequency and phase-lock the frequency sources to a stable reference frequency. Deacon et al. utilized PLLs at 25 GHz and 26 GHz to drive separate cascaded EO-combs, consisting of an intensity modulator EOM in series with a phase modulator EOM[8]. They used the phase stability of a PLL to decrease the noise of dual comb spectroscopy, providing further motivation for utilizing PLL architecture for driving the combs. To the best of our knowledge, this is the only other laser using PLLs to stabilize the frequency and phases of the driving frequencies.

The comb outlined in this chapter has a > 120 GHz comb bandwidth and 80 MHz comb tooth spacing (repetition rate), which creates a comb that will be useful in spectroscopy and metrology. Like many other EOM-based combs,

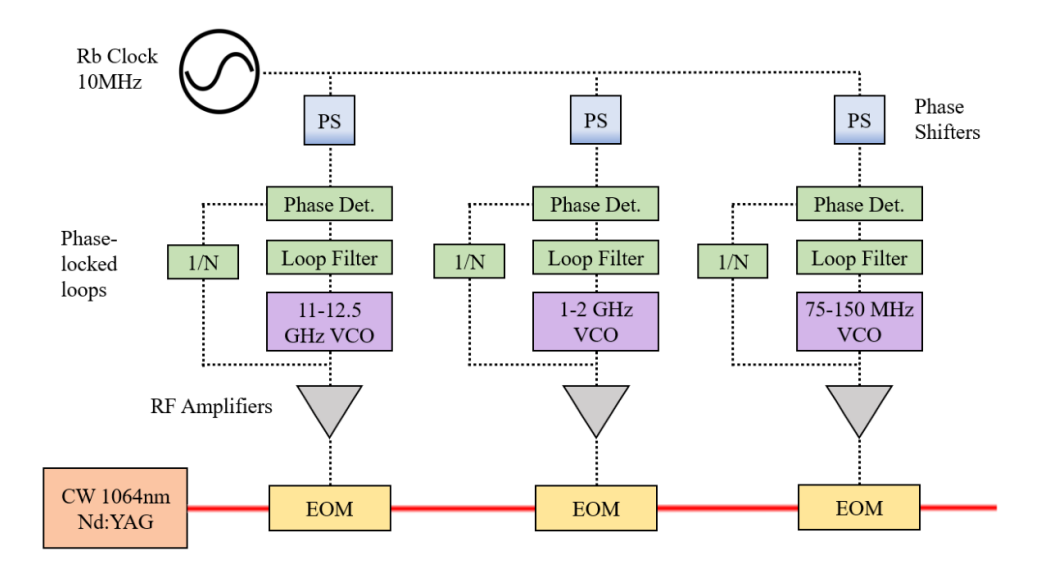


Figure 2.1: EO-comb Architecture and electronic block diagram, full details in text. PS is a phase shifter, Phase Det. is the phase detector or phase comparator, VCO is a voltage controlled oscillator, and 1/N is a frequency divider[13].

this one could also be further broadened in a nonlinear fiber and amplified. The organization of this chapter is as follows. Section 2.1 describes the EO-comb in detail, and the methods used to characterize the comb, section 2.1.3. The tests of the RF electronics and the optical comb characterization is in section 2.2. A discussion of the sideband intensities is found in section 2.3.

2.1 Electro-Optic Comb Architecture

2.1.1 RF Components

The frequency sources for the EOMs are phase and frequency stabilized to a single, stable frequency source through the use of phase locked loops (PLLs). A detailed circuit diagram and layout is shown in appendix A.I, but will be described here. The reference frequency is a 10 MHz Rubidium (Rb) clock (SRS SIM940). Three phase shifters (Synergy Microwave PK-721S) are set before the PLLs to provide relative phase control of each driving frequency. The PLLs are comprised of a phase frequency detector or phase detector, a loop filter, voltage controlled oscillator (VCO), and a frequency divider. The VCO is set to the desired frequency then output to both an amplifier and a frequency divider. The frequency division achieves frequency matching between the VCO frequency

that drives the EOM and the Rb clock and is adjustable. The 75-150 MHz PLL (Analog Devices ADF4152HV) includes as the phase comparator and loop filter and interfaces with an external VCO (Minicircuits ZOS-150+). The 1-2 GHz PLL uses the same PLL board but the VCO is the on-board VCO. The 11-12.5 GHz PLL uses a different PLL (Analog Devices ADF41020), again utilizing the onboard VCO. The PLL output voltages are amplified individually using: II-12.5 GHz (MiniCircuits ZVE-3W-183+), I-2 GHz (Minicircuits ZVA-183WX-S+), and 75-150 MHz (Minicircuits ZHL-2010+). The amplified frequencies are then sent to their respective EOM. The three EOMs used are: 11-12.5 GHz (EOspace PM-DS5-10-PFA-PFA-106-LV), 1-2 GHz (IXBlue NIR-MPX-LN-10 0-10 GHz), and 75-150 MHz (IXBlue NIR-MPX-LN-2 0-2 GHz). The frequencies are set to be exact harmonics of the lowest frequency, within the precision of the frequency divider control. The frequency spacing of the EOMs was chosen to maximize the sidebands produced by each EOM while staying below the RF damage threshold of the EOM, with 13 harmonics between the two lowest frequencies and 11 harmonics between the highest two frequencies.

2.1.2 Optical Components

The EO-comb uses a cascaded architecture consisting of three phase modulators in series, pictured in Fig. 2.1. The seed laser is a CW Nd:YAG (Coherent Mephisto) with ≤ 3 kHz optical linewidth at 1064 nm. The seed light is coupled into polarization-maintaining fiber and sent through three EOMs in series, starting with the one driven at the highest frequency, and subsequent EOMs driven at a lower frequency. The EOMs are all fiber-coupled, waveguide-type with polarization-maintaining couplers that join the fibers from each EOM in series. The diagnostics and characterization optics are all done in free space.

2.1.3 Comb Characterization Methods

The PLL outputs are fairly simple to characterize since it is just RF sin waves. Depending upon the EOM and amplifier combination, some attenuation is needed to prevent damage. The highest frequency PLL is hardest to characterize, the phase noise and signal can be observed using a 8x frequency divider (Lotus Communications FD8DC18G) and a spectrum analyzer. The output power can be quantified using a Analog AD8317 evaluation board, which converts a RF sin wave to a proportional DC level. Through these quantification methods a 7dB attenuation is used before the highest frequency amplifier. The second highest PLL 1-2 GHz can be quantified using the spectrum analyzer and a RF power meter (Crystek CPDELTS-4000). This frequency requires 2 amplifiers

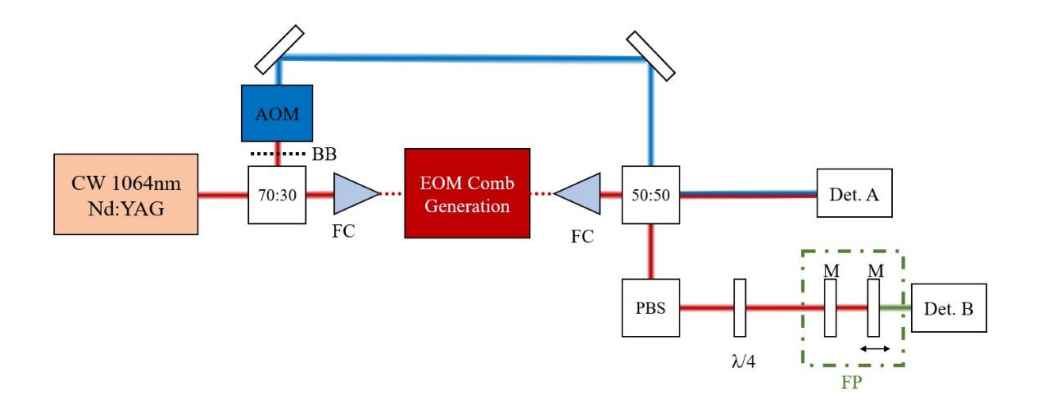


Figure 2.2: Detection Scheme. 70:30 and 50:50 are beam splitters of the same ratio. PBS is a polarizing beam splitter. BB is a beam block that is placed during Fabry-Perot spectra collection. BD is a beam dump. FC are fiber couplers. FP is the Fabry-Perot Cavity. Det A. collects the Heterodyne measurement data. Det. B. collects the Fabry-Perot Spectra[13].

and 14 dB of attenuation after the first amplifier. The lowest frequency PLL has an external VCO (pictured in Fig A.2), this sin wave is the easiest to quantify due to the lower frequency. The output from the power splitter is not attenuated when sent to the respective amplifier. Each VCO will output harmonics of the fundamental frequency, these frequencies are not filtered out in this experiment since they do not detrimentally affect the resultant EO-comb.

To characterize the comb spectra in the RF, both in frequency and phase, it is necessary to beat the comb against another frequency source to separate each comb tooth in frequency to individually detect it on an RF spectrum analyzer. Comb frequencies are rigorously described the carrier envelope offset frequency, f_0 and the repetition rate, f_{rep} such that the optical frequency of each n^{th} comb tooth is $v_n = f_0 + n f_{rep}$. Then comb is beat with a frequency shifted portion of the CW Nd:YAG laser, $v_{YAG} + f_{AOM}$. The comb teeth are unidentifiable with their distinct beat frequencies of the n_{th} comb tooth, b_n by $b_n = v_n - (v_{YAG} + f_{AOM}) = f_0 + n f_{rep} - (v_{YAG} + f_{AOM})$. The 80 MHz modulation and the first mode of the 1.04 GHz modulation fall within the bandwidth of the RF spectrum analyzer, which is 1.5 GHz. The 11.44 GHz data was obtained by dividing the signal by eight.

The optical layout is shown in Fig. 2.2). To detect each comb tooth, a portion of the CW Nd:YAG laser is split off and sent to an AOM driven at 260 MHz (Isomet M1250-T260L-op45 and 536F-L). The frequency shifted

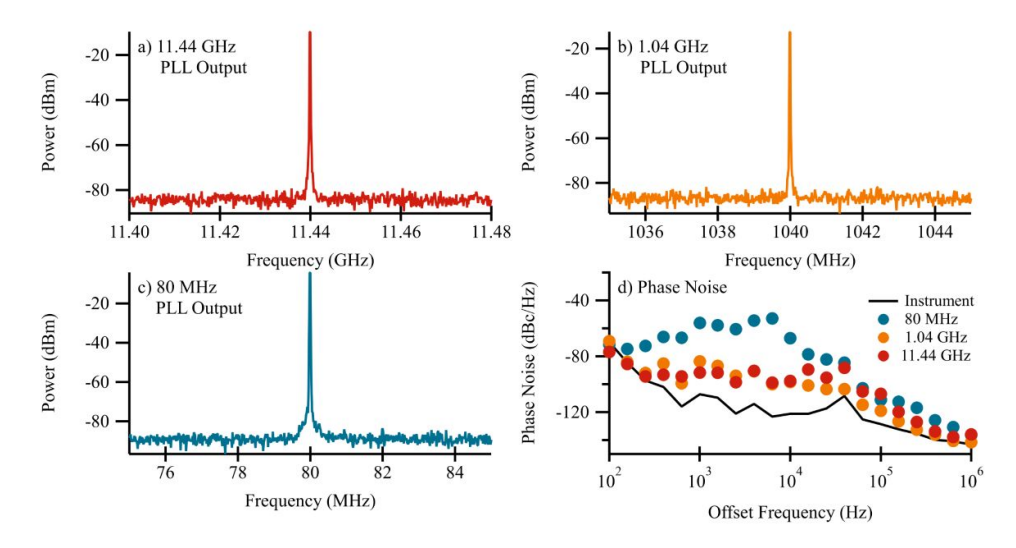


Figure 2.3: a) RF Spectra of the II-I2.5 GHz PLL at II.44 GHz b) RF Spectra of the I-2 GHz PLL at I.04 GHz c) RF Spectra of the 75-I50 MHz PLL at 80 MHz d) Phase noise of the RF sources. The II.44 GHz source was divided by 8 to collect this data[I3].

Nd:YAG is then made co-linear with the EO-comb and focused onto a detector (Coherent ET-3000) for heterodyne detection. The resultant RF spectrum is amplified with an low noise amplifier (Pasternack PE15A1007), and collected by a RF spectrum analyzer (Rigol DSA815) for frequency measurements and a second RF spectrum analyzer for phase noise analysis (Advantest R3267).

A custom program was written in LabVIEW to collect the full RF spectrum (see Appendix Section A.I). The spectrum analyzer (Rigol DSA815) can be interfaced using standard serial connection, and can be remotely controlled. The spectrum analyzer will only collect 600 data points of a scan, regardless of the frequency span or RBW. To fully capture and discriminate the frequency modes of the EO-comb, the span was decreased. For the data shown in this chapter a span of 180 kHz with a RBW of 300 Hz was chosen. This means the data point spacing matched the RBW. However the desired span and RBW could be controlled in the program. An important consideration for using this program is choosing how long the program pauses to allow for the spectrum analyzer to collect a full spectrum. This required around 5 percent more time than the sweep time of the spectrum analyzer, for example a 2 second sweep would require a 2.I second pause to complete a full sweep.

To quantify higher frequency modulations and the EO-comb optical spectra, a home-built scanning Fabry-Perot spectrometer is used, as shown in Fig.

2.2. The Fabry-Perot consists of two highly reflective planar mirrors (R > 0.9995, Edmund Optics 89-452) mounted with one mirror on a translation stage controlled by a stack piezo (Thorlabs PC4GR). The piezo is controlled by a high voltage amplifier (Thorlabs MDT694B) and a function generator (Rigol DG1022Z). The light was detected with a large mode area detector after the second mirror (Det B: Thorlabs PDA10A2). The spectra was collected and saved with an oscilloscope (Sigilent SDS2352X-E). A quarter waveplate and polarizing beamsplitter placed before the Fabry-Perot act as an optical isolator preventing the reflected light from heading back to the laser.

The Fabry-Perot was designed to observe the high frequency modulations and collect the full optical spectrum of the EO-comb. The finesse (>500 typ.) was verified by measuring the line-width of the Nd:YAG, which has a specified line-width ≤ 3 kHz, much lower than the FWHM of the cavity. In our work, we were not able to resolve individual comb teeth, at the highes FSR. The free spectral range was varied from as low as 2 GHz, to measure the 80 MHz spectra, to about 175 GHz, for the full spectrum.

2.2 Electro-Optic Comb Performance

Figure 2.3 shows the RF spectra, panels a) - c), and phase noise, panel d), at the output of each PLL, with the phase noise collected after amplification. The PLLs are providing the necessary stable, driving frequencies for the EOMs, at the set desired frequencies. There are no additional frequencies being sent to the EOMs, with the exception of some intensity in the higher harmonics. The phase noise of the 80 MHz output is higher than the other PLL outputs, until approximately 100 kHz. This is perhaps not surprising since that PLL is not specifically optimized for 80 MHz, while the PLLs for the other two frequencies were optimized for the driving frequency used. The instrument response of the phase noise was taken with the Rb clock.

The RF spectra of the laser is obtained by recording the heterodyne beat with the 260 MHz AOM-shifted seed laser. Figure 2.4 shows the RF spectra of the seed laser and 80 MHz modulation only. What intensity remains of the unmodulated seed laser, labeled as the 0^{th} sideband, shows up at the 260 MHz modulation frequency. The 80 MHz modulation creates 17 observable modes in the positive direction, and at least 15 in the negative direction. This is sufficient modulation to span the 1.04 GHz sidebands, corresponding to the 13^{th} sideband from the preceding EOM. The inset zooms in on the $+3^{rd}$ sideband on a log scale so the noise and peak shape are visible. The peaks visible in the

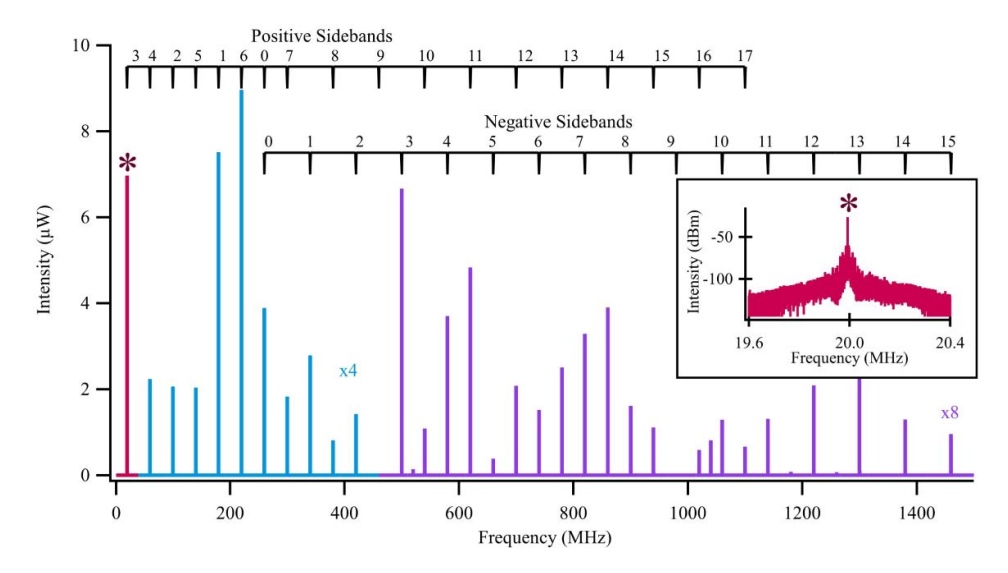


Figure 2.4: RF Spectra of the Nd:YAG seed laser with only the 80 MHz EOM Modulation on beat with the 260 MHz AOM modulated laser. Racetracks denote the positive and negative modulations referenced from the seed laser. The unmodulated seed laser is the 0^{th} mode. The light blue section of spectra is multiplied by 4, the purple section multiplied by 8, and the I/f noise removed for clarity[13].

spectra and not assigned as peaks from the 80 MHz modulation are harmonics of the AOM driver.

Figure 2.5 a) is the AOM beat RF spectra for the Nd:YAG with just the 1.04 GHz EOM turned on (pink), and for the full comb with all three EOM's turned on (gray). The full EO-comb is, offset by 0.5 mW for clarity and the sideband numbers labeled with the racetracks. The "0" label corresponds to the unmodulated Nd:YAG laser frequency, ν_{YAG} , such that the positive 3^{rd} comb tooth frequency, for example, is at 240 MHz ($\nu_{YAG} + 240MHz$) and shows up at 20 MHz in the heterodyne RF beat spectrum. The pink trace shows the optical beat spectra in the RF when only 1.04 GHz EOM is turned on. The positive 13^{th} sideband overlaps with the 1.04 GHz modulation, as expected. Note that with the linear scale the noise is not visible.

The phase noise is reported in Fig 2.5 b), of the full EO-comb, the AOM modulated Nd:YAG laser, 1.04 GHz modulation only, 80 MHz modulation only, and the instrument response. The phase noise of the full comb is greater from 1 kHz to 600 kHz that in either the 80 MHz or 1.04 GHz sources. Since we could not directly measure the phase noise of the 11.44 GHz modulation with our spectrum analyzer, the increase in phase noise can possibly be attributed to

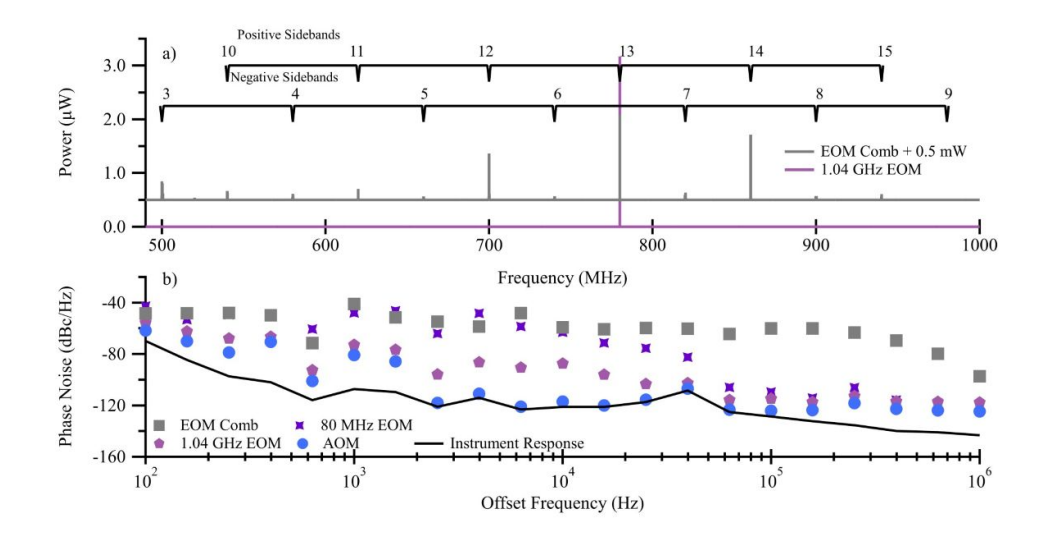


Figure 2.5: RF Spectra a) Selection of the RF Spectrum from 490-1000 MHz, The EO-comb signal is shifted up by 0.5 mW. The racetracks denote the comb tooth number from the seed laser for the positive and negative sides of the EO-comb. b) Phase noise of the instrument (black line), AOM modulated seed laser (blue circle), single modulation at 1.04 GHz (pink circle) and 80 MHz (purple square), and the full comb (gray square)[13].

the II.44 GHz and/or optical phase noise. The RF bandwidth of the spectrum analyzer (I.5 GHz), detector (2 GHz), and LNA (3 GHz) limit the amount of comb teeth that are observable. To measure the higher frequency modulations, the home-built Fabry-Perot spectrometer was used.

The full spectra of the EO-comb, II.44 GHz modulation, and I.04 GHz modulations were recorded with the scanning Fabry-Perot spectrometer, as seen in figure 2.6. Fig. 2.6 a) shows the modulation with only the II.44 GHz EOM on. The first modulation at II.44 GHz creates 5 frequency modes on either side of the fundamental, which gives the EO-comb its optical bandwidth. Fig. 2.6 b) is the Fabry-Perot spectra of the laser with only the I.04 GHz EOM. The intensity profile of each modulation is discussed in section ?? and consistent with EOM modulation of a single frequency and the first few harmonics, as expected. Fig. 2.6 c) shows the Fabry-Perot spectrum of the entire EO-comb laser. Individual comb teeth are not resolved, as expected, however intensity is shown across >120 GHz of bandwidth. This optical bandwidth is much greater than many EO-combs with Megahertz or lower repetition rates, before external broadening [31, 30, 41, 19, 18].

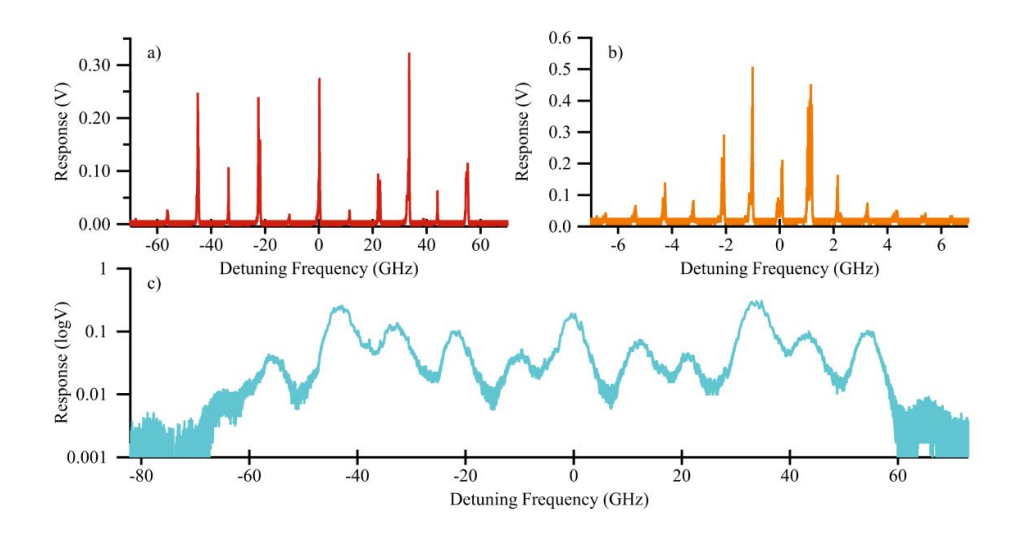


Figure 2.6: Fabry-Perot Spectra a) seed laser modulated at 11.44 GHz b) seed laser modulated by 1.04 GHz c) The spectrum collected of the full EO-comb, averaged 3 times[13].

To demonstrate the overlap of the sidebands as a result of the harmonic modulation frequencies, Fabry-Perot spectra are taken with and without harmonic modulation for comparison, Figure 2.7. The EO-comb with only 1.04 GHz and 11.44 GHz modulation, the 11^{th} harmonic, are shown in Figure 2.7a) with racetracks counting sidebands from the unmodulated peak, set as o GHz. The -11^{th} 1.04 GHz sideband overlaps with the first 11.44 GHz sideband, as expected. The line-shape of each frequency mode is from the scanned Fabry-Perot and not the line-shape of the EO-comb. The laser with only 11.44 GHz EOM modulation is shown in panel c) for reference. EOM modulation with 1.2 GHz and 11.44 GHz, not a harmonic frequency, is shown in panel b). The 1.2 GHz modulation sidebands on adjacent 11.44 GHz sidebands do not overlap or fill in the gap between 11.44 GHz modulations. The intensities of the harmonically overlapped peaks compared to the non-overlapping peaks between the 11.44 GHz modulations shows the second advantage of the harmonic modulation scheme. The intensities of the sidebands from adjacent 11.44 GHz modulations adds in the harmonic modulations scheme, especially clear when comparing the "-7" sideband from panel a) to the "-7" sideband in panel b).

The EOM modulation does not seem to appreciably affect the relative intensity noise (RIN) (see Figure 2.8). There are various frequency spurs in the seed laser RIN, and are not a result of the EO-comb generation. The baseline is not continuous because the data is stitched using different amplifiers, which

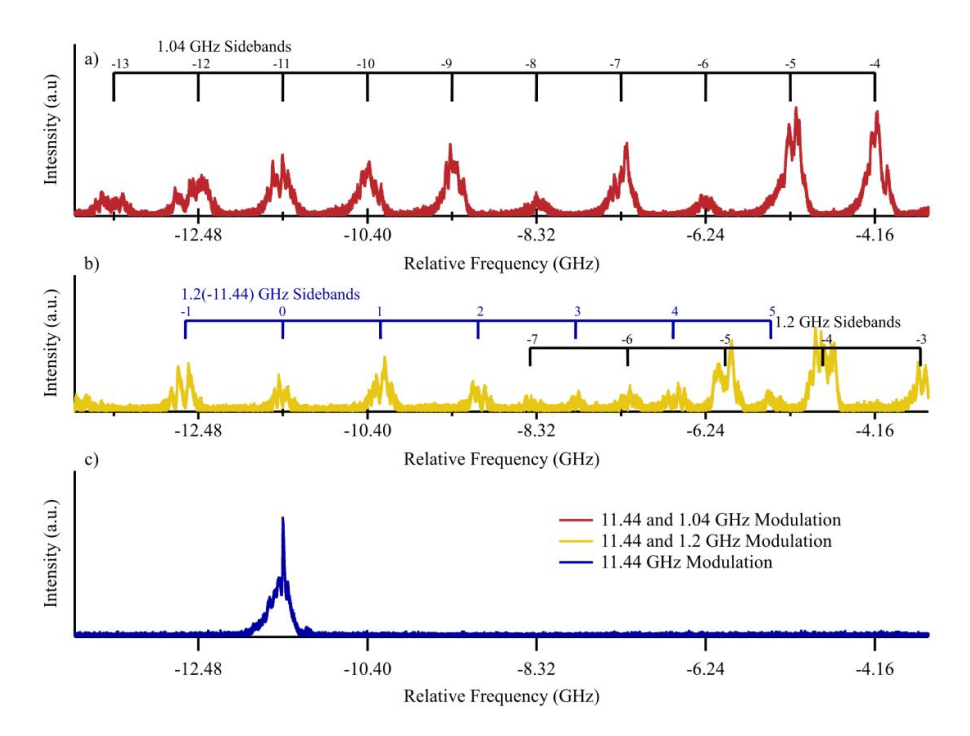


Figure 2.7: Fabry-Perot Spectra a) Trace of II.44 and I.04 GHz modulation. The harmonic numbers are measured from the seed laser which is set to 0 GHz. b) Trace of the II.44 and I.2 GHz modulation. The black racetrack is counting I.2 GHz modes starting at the seed laser. The blue racetrack is counting modes generated from the -II.44 GHz mode. The peak width is limited by the Fabry-Perot cavity and is not a measure of the comb tooth width [13].

changed the noise floor; the higher frequency data starting at 1 kilohertz used a LNA and a different spectrum analyzer. Since the RIN is unaffected by the EO-comb generation, lower noise seed laser can be used to reduce the RIN.

2.3 Sideband Strength with Harmonics

The conventional discussion of EO-comb generations uses the Bessel function to describe the intensity of the side-bands generated by a single phase modula-

tion at frequency Ω . This modulation is symmetric about the seed laser:

$$E_{out} = Acos(\omega t - \delta sin(\Omega t))$$

$$= A[J_0(\delta)cos\omega t + J_1(\delta)cos(\omega + \Omega)t + J_1(\delta)cos(\omega - \Omega)t + J_2(\delta)cos(\omega + 2\Omega)t + J_2(\delta)cos(\omega - 2\Omega)t + J_3(\delta)cos(\omega + 3\Omega)t + J_3(\delta)cos(\omega - 3\Omega)t + J_4(\delta)cos(\omega + 4\Omega)t + J_4(\delta)cos(\omega - 4\Omega)t + ...]$$
(2.1)

 E_{out} is the electric field of the modulated seed laser[46]. The amplitude of each mode is described by Bessel function, $J_n(\delta)$, the n being the side-band number and δ is the phase modulation index. The phase modulation index is defined as $\delta = (1/2)\pi(V/V_\pi)$. This solution does not account for multiple frequencies in a single phase modulator. The driving modulations in this work included higher order harmonics inherent to the frequency sources. The output electric field in this work is described in equation 2.1. The equation can be extended to

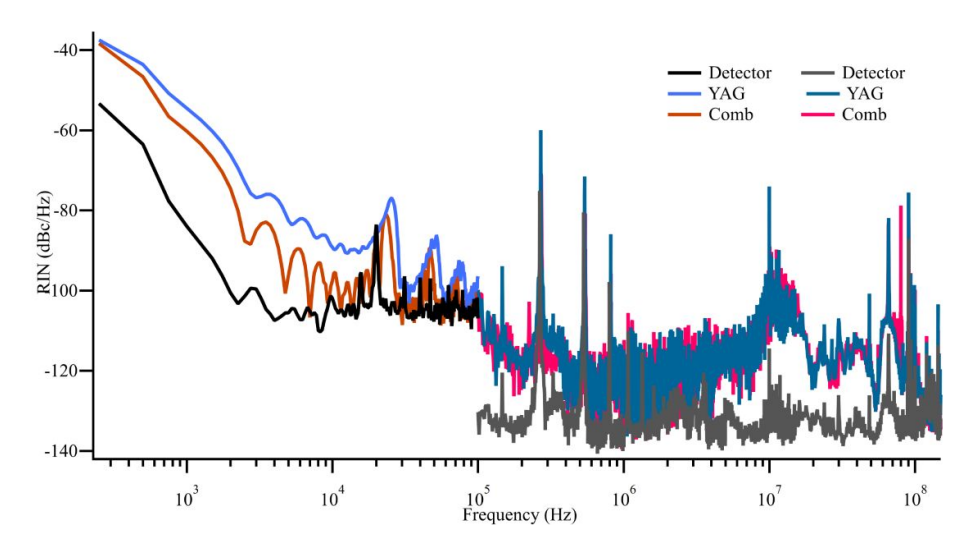


Figure 2.8: RIN collected of the background, YAG seed laser, and the EO-comb. For frequencies higher than 1 kHz, a low-noise amplifier (LNA) was used after the detector to increase the signal above the detector noise floor. The RIN is dominated by the Nd:YAG seed laser[13].

have any amount of harmonics.

$$E_{out} = Acos[\omega t - \delta_1 sin(\Omega t + \phi_1) - \delta_2 sin(2\Omega t + \phi_2) - \delta_3 sin(3\Omega t + \phi_3) - \delta_4 sin(4\Omega t + \phi_4)...]$$
(2.2)

The phase modulation index changes with frequency because V_{π} is frequency dependent. This model of the electric field predicts asymmetric side-bands strengths, with the intensities depending upon the phase modulation index of each harmonic and the phase of each harmonic. This predicted intensity pattern is consistent with the asymmetric sideband observed in figures 2.6 and 2.4.

CHAPTER 3

CONSTRUCTION OF A DUAL COMB SPECTROMETER

Dual Comb spectroscopy is a high resolution technique that is able to resolve the intensities of individual comb teeth. The lasers described in chapter 2 and this chapter are both in the near infrared (NIR), to achieve comb tooth resolution without dual comb would require expensive instrumentation like a virtually imaged phase array (VIPA) spectrometer. This style of spectrometer has similar resolution to dual comb however is more expensive and slower acquisition rate. This chapter will explore the development and design of a dual comb spectroscopy experiment with mismatched combs. The first section will be the construction of the second frequency comb. The second will be the construction of the dual comb experiment.

3.1 Constructing Yb Oscillator

The first laser that will be used for the dual comb experiment is described in depth in chapter 2. However a second frequency comb needed to be built. The Ytterbium (Yb) fiber oscillator has been built 2 other times in the Reber lab, and will be referred to as the oscillator. The oscillator is a frequency comb that has intensity centered around 1040 nm. This oscillator was built to match the lasers used in other experiments in the Reber lab; so that an initial dual comb experiment could be performed while work continues on the other experiments [7]. The comb starts at the 976 nm pump diode which provides the initial energy for the laser. The pump diode is introduced to the cavity through the wave division multiplexer (WDM), which introduces the 976 nm light into the cavity but does not allow the desired wavelengths out. Then the pump light travels through the Yb-doped fiber which generates the >1000 nm light. The

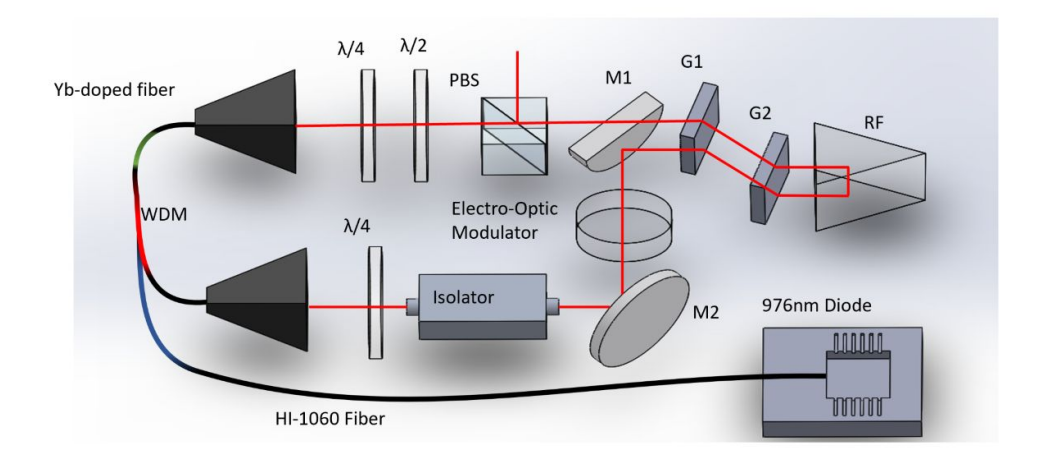


Figure 3.1: This is a diagram of the laser cavity of the Yb fiber oscillator. WDM is a wave division multiplexer. $\lambda/2$ and $\lambda/4$ are half and quarter waveplates respectively. PBS is a polarizing beam splitter. G1 and G2 are 600 lines/mm gratings. RF is a retroreflector. M1 and M2 are protected silver mirrors.

light is then output into free space and travels through a quarter and half waveplate. The next optic is a polarizing beam splitter (PBS) which is the output coupler for the laser cavity. Then the light travels through the grating pair and retro-reflector which controls for the second order dispersion in the cavity. The light reflects off of the first mirror and travels through an EOM. The light then travels through an isolator to ensure that the light only travels in one direction. Then there is one last wave-plate before the light is coupled back into fiber to complete the laser cavity.

The oscillator is passively mode-locked by adjusting the wave-plates within the cavity. While the f_{rep} and f_0 are fairly stable for the oscillator, it does shift slowly over time. The first control is a ring piezo that is attached to the first grating, by changing the position of the first grating the f_0 can be tuned. The repetition rate can be changed by applying a voltage to the EOM which changes its refractive index and changes the length of the cavity. Through these two controls the absolute position of the frequency modes can be stabilized. The final oscillator has a repetition rate of 72.3 MHz with a wide optical bandwidth. The laser was locked so that the oscillator has more intensity at 1064 nm, an example spectrum is shown in Fig 3.2.

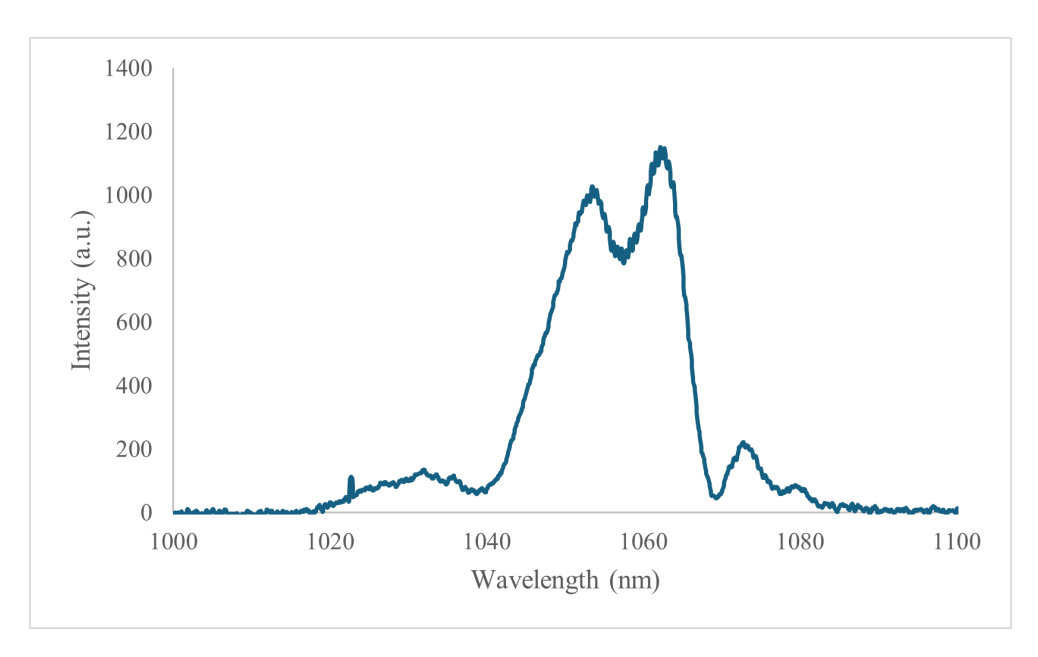


Figure 3.2: This is a spectrum of the oscillator. This lock was chosen due to the high intensity around 1064 nm.

3.1.1 Controlling f_0 and f_{rep}

First we will discuss the tuning bandwidth of the repetition rate. The EOM was driven using a high voltage amplifier (Thorlabs HVA200), the driving voltage was sent to a DC value and the repetition rate was recorded using the frequency counter function of a spectrum analyzer (Advantest R3267). This was compared to a calculated change in path length from the EOM.

The change in path length was calculated using the equation $\Delta n = -1/2rn^3E$ from Boyd [3]. E is the strength of the electric field in V/m, and rn^3 (electrooptic coefficient) was estimated from the crystal type (33pm/V). This equation gives the change in the refractive index of the EOM and that can be used to calculate the change in path length of the laser cavity. The length of the EOM crystal and electro-optic coefficient were estimated from available values, which were not specified by the manufacturer. Even with these inconsistencies there is general agreement between experimental and calculated values. This test also shows that the oscillator repetition rate can be tuned ± 20 Hz, which is the capture range of the repetition rate lock.

The f_0 has a separate tuning range and bandwidth from the repetition rate control. Similar to the repetition rate capture range, a DC level can be sent to the ring piezo attached to the first grating. This gave a tuning coefficient of

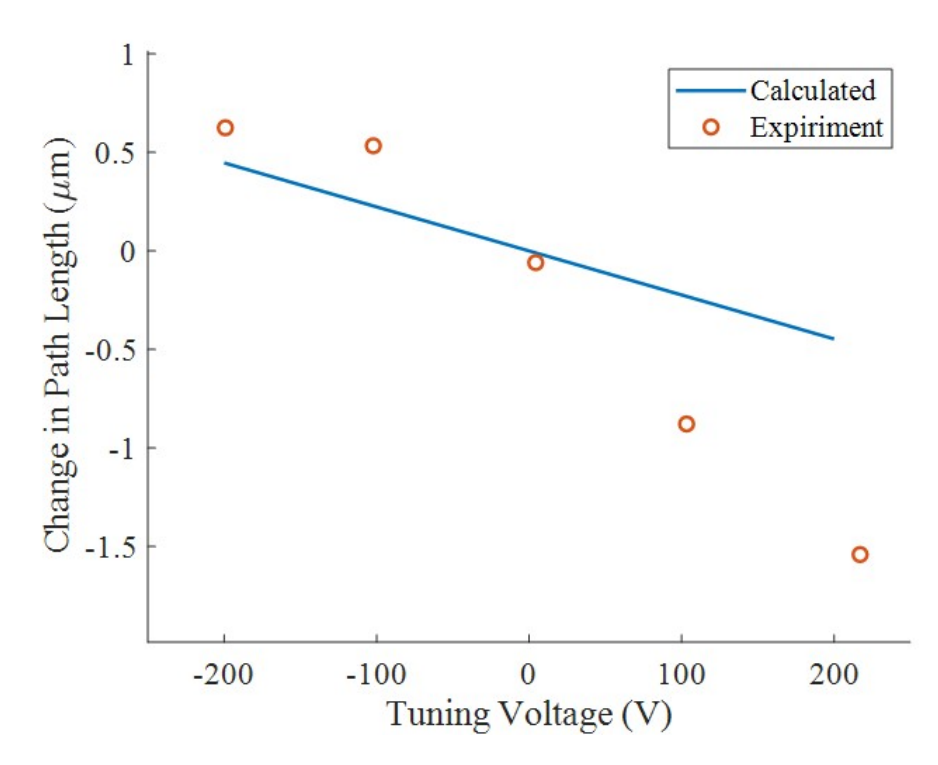


Figure 3.3: The solid blue line is the calculated change in path length. The orange circles denote experimental changes in path length of the oscillator.

o.1 MHz/V, which gives a capture range of 15 MHz. This is dictated by the maximum voltage of the ring piezo (150 V). This capture range was collected with DC levels and is not indicative of how well the ring piezo can stabilize the f_0 . To test the modulation bandwidth of the actuator a triangle wave with a variable frequency was used to drive the ring piezo. This caused the beat note to oscillate in frequency. The broadening of the beat note was collected on a spectrum analyzer and processed afterwards. The code used to calculate the range of the beat note is in appendix A.2.1. The code took the average and standard deviation of the spectrum analyzer trace; Then found the range of frequencies that were above one standard deviation in power. The results of this treatment is shown in Fig 3.4, this data was taken over multiple days as well. The range decreases dramatically after 10 kHz, which is the modulation bandwidth. It is important to note that the triangle wave used to modulate the ring piezo had an amplitude of 11.25 V_{pp} . As the amplitude of the triangle wave increases the modulation bandwidth will decrease, however this data informs the design an implementation of f_0 stabilization.

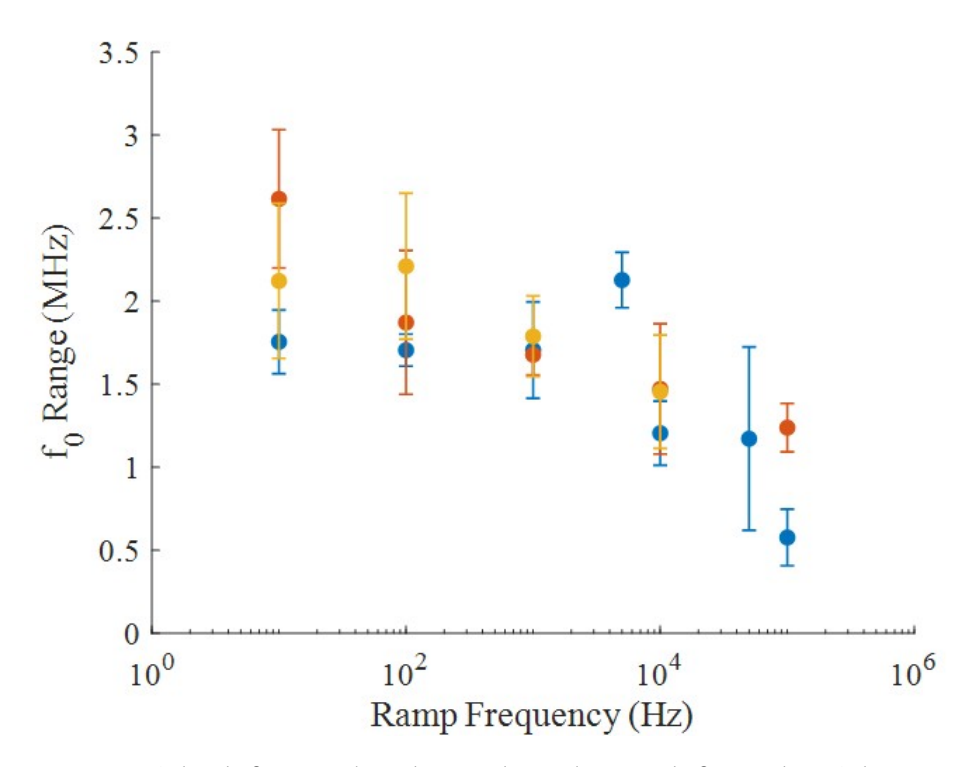


Figure 3.4: The different colors denote data taken on different days. The x axis is the frequency of the 11.25 V_{pp} triangle wave. The Y axis is the f_0 beat note range in Hz.

3.2 Dual Comb Spectrometer

The Dual comb experiment is relatively simple once both combs are constructed. The stabilization of the frequency combs will be discussed in the next section. The block diagram of the dual comb experiment is shown in Fig 3.5. The oscillator is output into free-space and compressed, before it is combined in a beam splitter and fiber coupled for the detection. The EO-comb uses the repetition rate of the oscillator as its reference frequency to stabilize the difference in the repetition rates. Before the EO-comb is generated some Nd:YAG light is fiber coupled and beat against the oscillator for the f_0 lock; the fiber coupled light was incident upon a detector (ThorLabs PDA015C2) with a bandwidth of 380 MHz. The detector signal is split into two pathways. The first pathway is low-pass filtered (Mini-Circuits BLP-50+) and the beat note is collected by the DAQ. The second pathway is sent to the f_0 locking electronics, which will be discussed in the next section. The EO-comb is generated in accordance

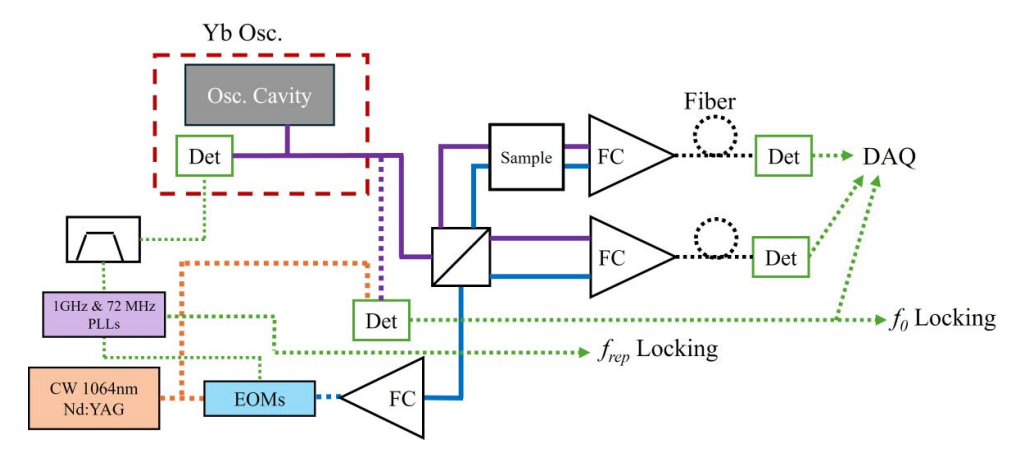


Figure 3.5: The dotted lines denote fiber optics. The solid lines are free-space optics. The dotted green lines denote RF connections. The oscillator and EO-comb are simplified for clarity. They are combined in free space and fiber coupled. The fiber coupled light is incident upon a detector that collects the sample and reference arms, and both signals are sent to the data acquisition board. The f_0 beat note is collected in tandem with the dual comb data.

with chapter 2. It is then output into free-space and overlapped with the oscillator and fiber coupled. The fiber coupled light is incident upon two matched detectors (Thorlabs PDAo₅CF₂). These detectors collect the dual comb interferograms, which have low-pass filters and DC blocks (Mini-Circuits BLP-44+ and Mini-Circuits BLK-89-S+) before it is sent to the DAQ. The raw detector signal is also monitored using an oscilloscope with a BNC T before the filter and DC block. For some interferograms, a higher bandwidth low-pass filter (Mini-Circuits SLP-90+) was used to reduce the power of higher frequencies to reduce anomalous frequencies in the dual comb spectra. The ammonia was placed in the signal arm/pathway by filling a 10 cm long stainless steel gas cell with AR coated windows (Cell: Thorlabs TMC510A, Windows: Thorlabs WG40530-C). The pressure of the gas cell was recorded using a pressure gauge (Kurt J. Lesker KJL300800). The interferograms are collected in time by a data acquisition instrument (Redpitya STEMlab 125-14 4 Channel) and Fourier transformed to resolve the beat frequencies of the dual comb signal. While the oscillator can be compressed to 100 fs. The characterization of ammonia will not be time resolved.

3.2.1 Oscillator Locking

When a frequency comb is locked the individual frequency modes will not move. Since dual comb can resolve the intensities of individual comb teeth, and not the absolute frequencies of the comb teeth. It is important to lock the frequency combs used in dual comb so the spectra can be resolved.

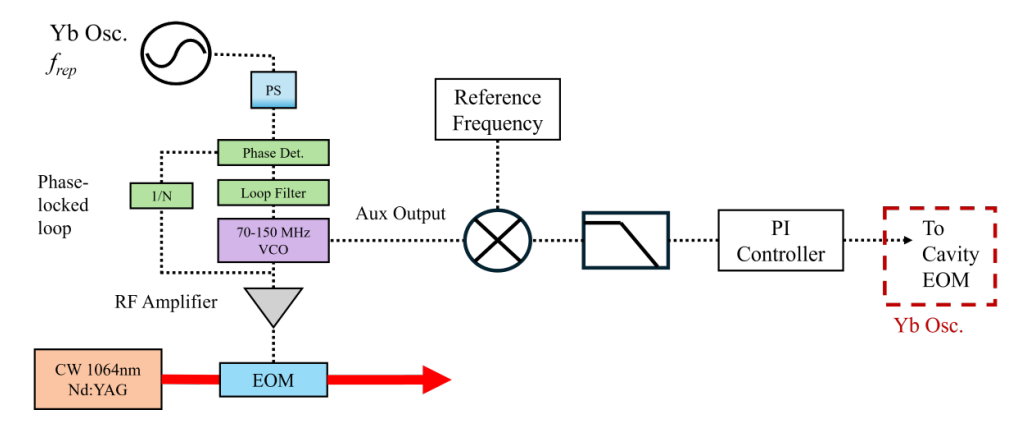


Figure 3.6: Repetition rate lock

The first lock that will be discussed is the repetition rate lock or the stabilization of the comb tooth spacing. This work is unique in that only one repetition rate lock is needed. The repetition rate lock is shown in Fig 3.6. The oscillator repetition rate can be monitored by a photodectector, this signal is band-pass filtered and used as the reference frequency to drive the PLLs that control the modulation frequencies. This ensures that difference in repetition rates is ensured. The auxiliary output of the lowest frequency VCO (Mini-circuits ZOS-150+) is mixed (Mini-circuits ZEM-M2TMH+) with a reference frequency from a function generator. The mixed frequency is filtered with a low pass filter (Minicircuits BLP-1.9+). This error signal is sent to a PI controller which modulates the driving voltage of the oscillator EOM. The oscillator EOM has a capture range of 40 Hz (see Fig 3.3), however the repetition rate is fairly stable. The function generator was selected so it can output a 70-80 MHz sin wave at 13 dBm of power. The power of the reference frequency is dictated by the power requirements of the mixer used. The low pass filter used in this experiment only has to effectively filter out the doubled repetition rate which is 140-160 MHz, and pass the desired signal which is less than 40 Hz. A low pass filter with a cut-off frequency of 2 MHz was chosen for this experiment, however an even lower cut-off frequency could be used.

Even if the repetition rate is stabilized, the f_0 can still move which is not desirable for high resolution spectroscopy. First lets discuss the stabilization of the EO-comb. The EO-comb by its design has a stabilized f_0 , this is because

the seed laser is temperature stabilized. This is not the case for all EO-combs, depending upon the stability of the seed laser used. We can use the stability of the Nd:YAG to help stabilize the oscillator. The fundamental Nd:YAG is heterodyned with the oscillator after a 1064 nm notch filter. The signal is filtered and amplified so a single comb tooth beat can be observed. This beat note is sent to an offset phase locked servo that can stabilize the f_0 . The output of this controller is used to modulate the grating ring piezo to lock the oscillator. The block diagram is shown in Fig 3.7. The locking frequency of the beat note and therefore the f_0 can be tuned by changing the reference frequency sent to the offset phase lock servo. An important design consideration for this locking scheme is how well you can isolate the single comb tooth beat note. A single comb tooth beat note is relatively weak compared to the harmonics of the repetition rate observed when a pulsed laser is incident on a photo-detector. There are two confounding factors when considering filtering a messy RF signal: first is the noise floor of the photo-detector used, and the second is the increase in baseline noise from rejected frequencies of the RF filters. The design of this style of lock will perform better when spurious frequencies are repressed as much as possible.

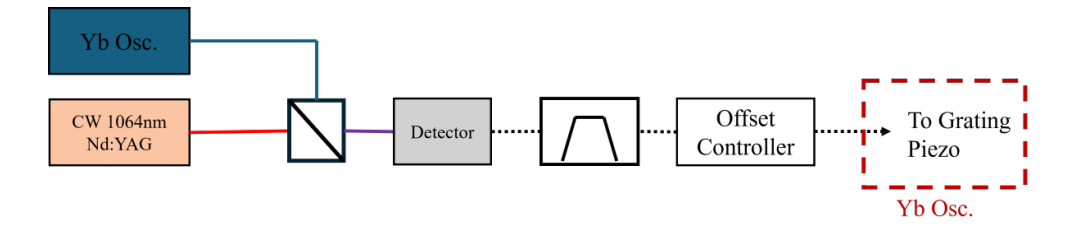


Figure 3.7: f_0 Locking scheme. After the detector multiple RF filters are used however just a band-pass filter is shown before the offset controller.

The block diagram in Fig 3.7 is simplified for clarity however it is necessary to fully explore the amplification and filtering of the f_0 beat note. The offset phase lock servo (Vescent D2-135) requires a minimum frequency of 240 MHz and a minimum power of -10 dBm. This means the beat note observed at -50 dBm will need to be amplified. The first step in conditioning the f_0 beat note is to use a low pass and high pass filter (low-pass: Mini-circuits BLP-250+, high-pass: Mini-circuits BHP-250+). The pair of filters remove most of the power outside of the desired 200-300 MHz band. Then this is amplified with a narrow band amplifier to increase the power. However there is still a high amount of signal from a harmonic of the repetition rate, so two band-pass filters (Mini-circuits SBP-240+) are used to attenuate the repetition rate. Then this is amplified again so the f_0 signal is above the -10 dBm requirement of the offset phase

lock servo. While the phase lock servo requires a minimum frequency, this has to be balanced with the bandwidth of the optical detector and the pass band of available band-pass filters. The bandwidth of the detector is simple to modify by choosing a detector with a higher bandwidth. The selection of the band-pass filters is the most challenging practical consideration. The harmonics of the repetition rate will be every 70-80 MHz and the f_0 signals will lie between those harmonics. This means a steep roll-off is required for this lock to work. The only available commercial filter with this steep roll-off within the frequency range of the phase lock servo and the detector is the SBP-240+ (Minicircuits). This filter has a pass band of 238-242 with a steep roll-off with the trade-off of 5 dB of attenuation in the pass band. This attenuation requires the two LNAs described earlier. When the oscillator was initially constructed it had a repetition rate of 74.5 MHz, which places the third harmonic at 223 MHz. Initially this did not seem like an issue; however with roughly 60 dB of gain from both LNAs and only 40 dB of attenuation from the pair of band-pass filters, the repetition rate signal was stronger than the beat note. So more path length in free-space was added to the oscillator, to achieve repetition rate of 72.3 MHz which increased the attenuation to 60 dB. This allowed for the repetition rate harmonic to be 2 orders of magnitude lower in power than the f_0 beat note. This allowed for the stabilization of the f_0 since a cleaner signal was being sent to the offset phase lock servo.

3.3 Data Collection

3.3.1 Time Domain Data Collection

The data collection of dual comb is not an insignificant challenge. The first consideration is the sampling rate of your chosen data acquisition card or instrument (DAQ). The minimum sampling rate needed is the repetition rate. Then the resolution or bit depth of the DAQ needs to be considered, a high resolution is desired at the trade-off of price. This led to the selection of the Redpitya STEM 125-14 4 input. It has a variable sampling rate with a maximum of 125 Msa/s. The sampling rate is controlled by the decimation, other manufacturers call it sparsing, which has to be a power of 2. When considering the sampling rate it is important to note that the Nyquist frequency is half of the sampling rate, which is the upper bound of the Fourier transform bandwidth. The Red Pitaya has a few different functions however the oscilloscope function is what is used in the dual comb experiment. There are 3 methods to collect dual comb data with the Redpitya. The first is the standard oscilloscope function

tions, these can be controlled with Matlab or similar software, which was used to collect the ammonia spectra. This method allows for adjusting the sampling rate, the gain of each channel and allows you to collect 4 channels simultaneously (see Appendix Section A.2.2). The draw backs are that each channel is limited to 2^{14} (16384) data points and one channel must have a waveform that can be used to trigger. The second method is called deep memory acquisition or DMA, this method is similar to the standard oscilloscope function (see Appendix Section A.2.3. However, it stores the data in the memory of the DAQ which slows down the acquisition. The DMA acquisition can collect up to 2^{21} data points, however there is a phase slip every 2^{19} data points which indicates that this method is not continuous in time. This method also does not have support to collect data on 4 channels simultaneously, or the documentation is lacking for this use case. The last method is data streaming, the sampling rate is limited to 31 Msa/s however up to 2 billion data points can be collected. The lower sampling rate is the primary reason this method is not used for this work.

3.3.2 Fourier Transform and Spectra Generation

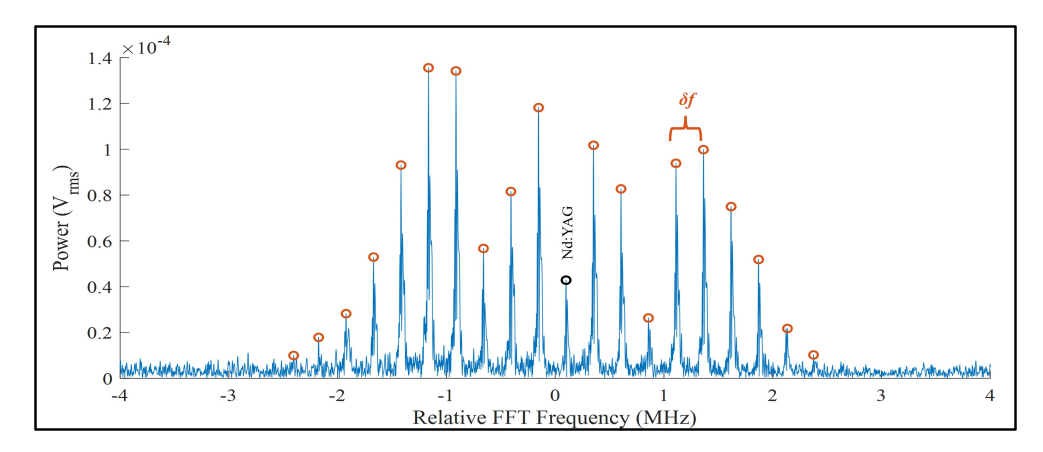


Figure 3.8: The blue curve is the Fourier transform of the time domain data. The black circle denotes the beat note of the fundamental Nd:YAG. The orange/black circles denote the data points that would be collected for constructing the spectrum.

The Redpitya acquisition board collects time domain data, however this must be converted to the frequency domain to interpret the spectra. The code used to perform the Fourier transform and retrieve the intensities and positions of the comb tooth pairs beat notes is in Appendix Section A.2.4. An example Fourier transform of the lowest frequency PLL and EOM is shown in Fig 3.8. The repetition rate and f_0 were stabilized in this spectrum. The δf was set

to 250 kHz for this interferogram. Peaks are separated by the difference of the repetition rates and are centered around the Nd:YAG frequency. A channel of the Redpitya is collecting the unmodulated oscillator and Nd:YAG beat note, which allows for the assignment of the center of the dual comb spectra and is set to zero. To convert the frequency axis of the Fourier transform to optical frequencies, the Fourier transform peak position was multiplied by $f_{rep}/\delta f$. Once the center of the dual comb spectrum is set, the frequencies and intensities of the dual comb beat notes are collected on one channel. The second channel of dual comb does not use the peak picking algorithm; the beat note positions from the first channel are used to collect the power of the beat notes on the second channel. The frequencies and intensities from ten Redpitya traces are averaged together for one spectra. Then the baseline had to be corrected for, the transmission of one spectra was calculated by dividing the signal arm by the reference arm. To correct for differences in alignment and beat note intensities, the ammonia transmission spectra were divided by the transmission spectra of a background trace.

CHAPTER 4

AMMONIA SPECTROSCOPY

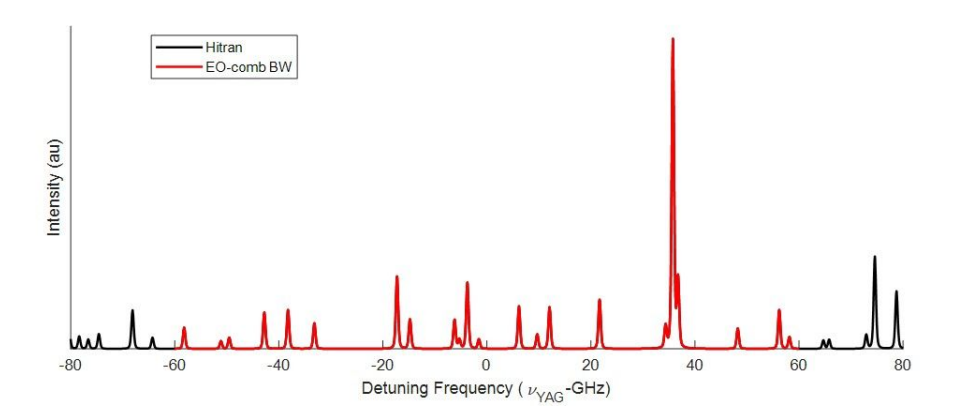
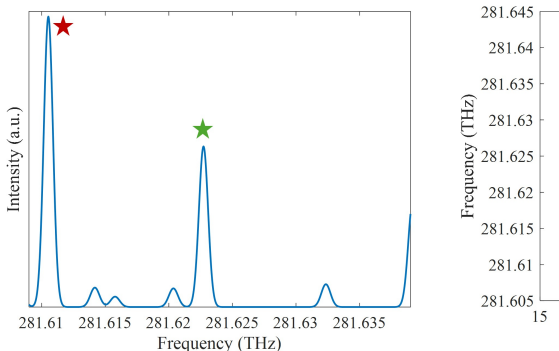


Figure 4.1: The black curve is a modeled NH_3 spectrum from Hitran. The red curve is the modeled bandwidth of the EO-comb.

Ammonia was chosen for the dual comb experiment because it is a gas at room temperature. The modeled spectrum is shown in Fig 4.1, the resolved modes in the spectral region is why a gas phase target was chosen. Ammonia is relatively weak absorber at these wavelengths, however if a NIR dye was chosen the broad transition might be indistinguishable from a flat decrease in intensity. For initial data collection only the two lowest frequency EOMs were used. This limits the optical bandwidth that can be resolved, but allows for easier assignment of dual comb beat notes. This allowed for spectra to be collected and shown in this chapter.

4.1 Nd:YAG Output Frequency Tuning

Since the EO-comb has limited band-with for these preliminary experiments, it was necessary to tune the center frequency of the EO-comb to resolve a spec-



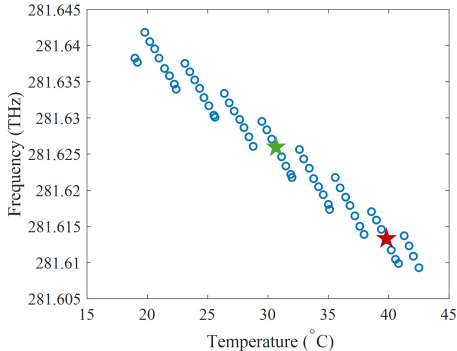


Figure 4.2: The left graphs is a selection of the modeled NH₃ spectrum. The right graph is the output frequency in THz of the Nd:YAG with crystal temperature. The color coded stars correspond to the two most intense transitions within the frequency tuning range.

tral transition. The Doppler broadened NH $_3$ spectrum and the Nd:YAG frequency tunability is shown in Fig 4.2. The spectrum is modeled from Hitran, with the transition intensity scaled to the absorbance cross section of the line. The Nd:YAG frequency tunability is retrieved from the specifications of the manufacturer. The higher intensity transition was chosen as an initial target, this corresponds to a Nd:YAG crystal temperature of 39.9°C. The controller is able to tune the crystal temperature easily, however this does not ensure that the Nd:YAG is outputting a single frequency. This needs to be monitored by the f_0 beat note. If the Nd:YAG is not outputting a single frequency it is shown by a doubling or widening of the beat note. If there is not single mode operation, the f_0 is not able to be stabilized and the EO-comb modes will split. These problems make it impossible to collect dual comb spectra.

4.2 Lineshape and Broadening

There are three sources of broadening that are applicable to ammonia in a gas cell. The first is lifetime broadening which is the broadening associated with the state lifetime as the name implies. A state with a long lifetime will have a narrow lifetime broadening. Ammonia's lifetime broadening was estimated by Foldes and coworkers to be under 90 MHz for transitions at 1.51 μ m [14]. While this work is located at 1.06 μ m, the lifetime broadening should be similar. The second source of broadening is Doppler broadening, which is caused from the translational movement of the ammonia gas. This is dependent upon the

temperature and mass of the molecule being interrogated. The equation used for this calculation was $\Delta\nu_D = 7.1 \times 10^7 \nu_0 \sqrt{T/M}$, $\Delta\nu_D$ is the FWHM of the Doppler broadening, ν_0 is the frequency of the transition in GHz, T is the temperature in kelvin, and M is the mass of ammonia in amu [2]. The Doppler broadening for ammonia at 298 K is 947 MHz. The last source of broadening is the pressure broadening, which has to be experimentally determined. Nouri et. al. quantified the pressure broadening at a variety of temperatures and pressures, which was used for the analysis in the next section [34]. For this work the pressure broadening FWHM is greater than 500 MHz. The dominant sources of broadening are from pressure and Doppler effects, the lifetime broadening is negligible at the temperatures and pressures in this work. The next consideration is that Doppler broadening has a gaussian line-shape and pressure broadening has a Lorentzian line-shape. These line-shapes need to be convoluted to create a Voigt profile which is the line-shape of the experimentally observed transitions (shown in Fig 4.3). This is necessary because the Doppler broadening FWHM is close to the FWHM of the pressure broadening.

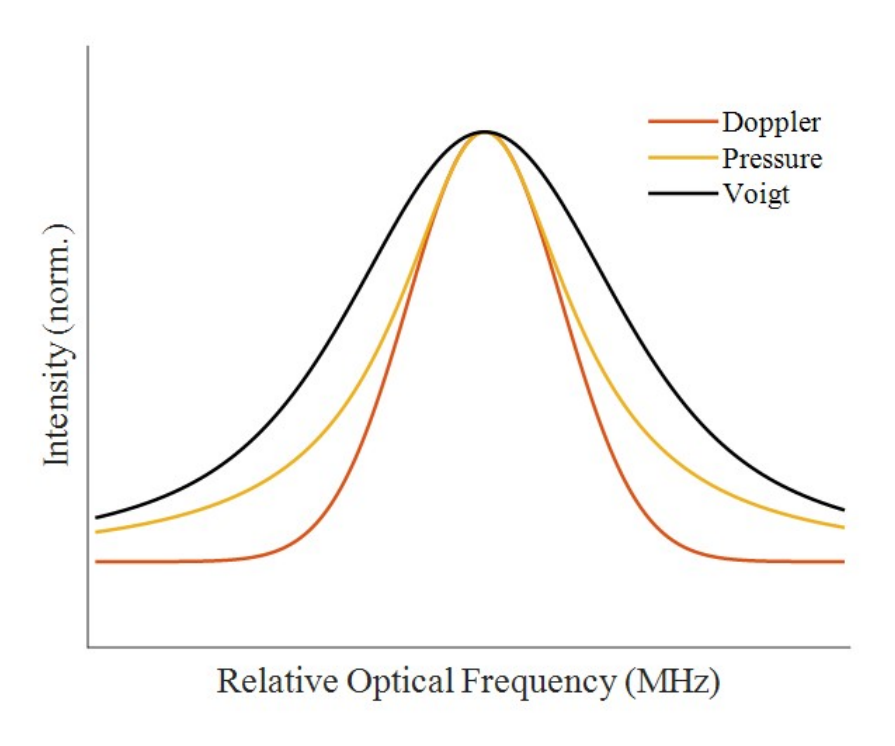


Figure 4.3: This figure depicts a convolution of the Doppler and pressure broadening line-shapes.

4.3 Dual Comb Spectra of Ammonia

Once the frequency of the Nd:YAG was tuned by the temperature dual comb spectra could be collected. The pressures of the gas cell were collected with a convection enhance pirani gauge. The ammonia spectra will be referred to by their cell pressure. The first day of data collection had a cell pressure of 248 Torr, the second day two different pressures were collected (150 and 52.1 Torr). The peaks observed on both of these days are shown in Fig 4.4. The second day of data collection the Nd:YAG had a slightly different temperature (0.02°C) so the transitions may not be the same. However the transitions observed with the 150 and 52.1 Torr spectra have the same center frequency which indicates they are the same transition. The 52.1 Torr spectrum also has a lower intensity, which matches Beers law predictions. The absolute frequency of the transition is unknown since dual comb gives relative optical frequencies due to the spacing of the comb teeth. To give absolute frequency accuracy and spectral assignments an external frequency reference like an atomic absorption line or a wave-meter is needed.

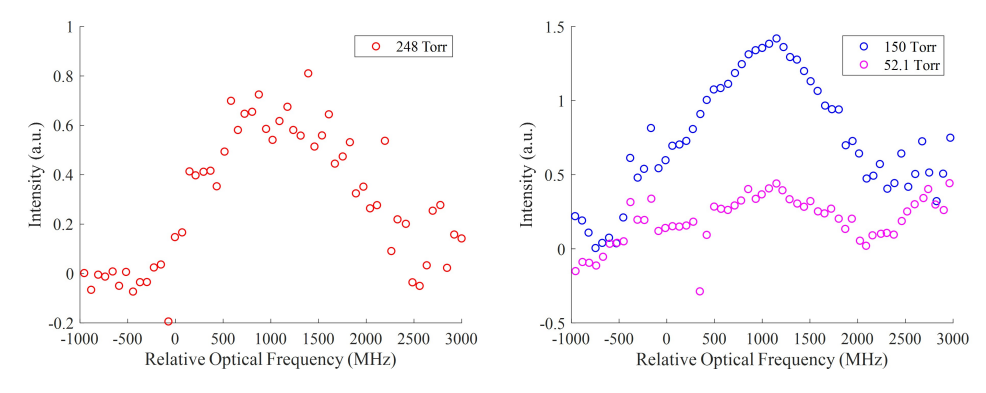


Figure 4.4: The left graph contains the peak with a cell pressure of 248 Torr. The right graph contains the peaks with cell pressures of 52.1 and 150 Torr. These data sets are not on the same graph because the Nd:YAG crystal was at different temperatures between these spectra, therefore it may not be the same ammonia transition.

The data shown is noisy however some analysis can be performed. To ensure that this singular peak is a transition of ammonia, a modeling of the line-shape was performed. The Doppler broadening FWHM was held constant at 947 MHz. Then the pressure broadening was modeled over a span and used to minimize the error in the data points above the FWHM of the spectrum, the code is shown in Appendix Section A.2.5. A full least squares fitting was not performed due to the noise in the baseline of the spectra.

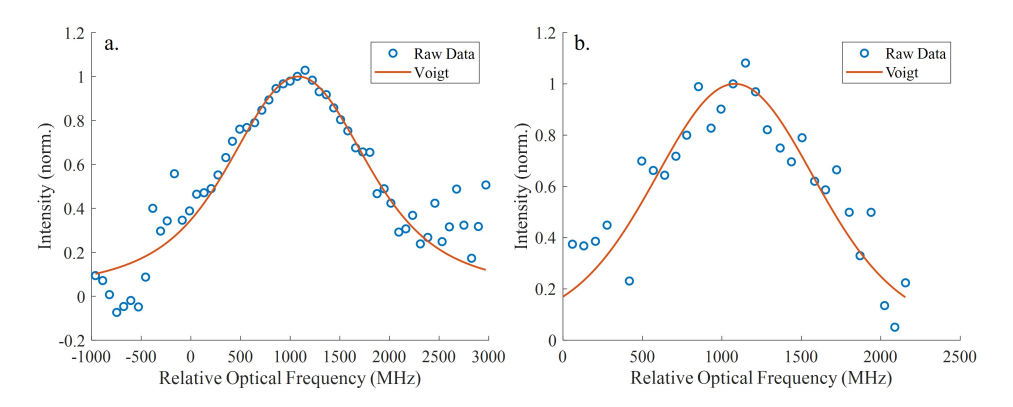


Figure 4.5: a) is the Voigt modeling of the ammonia spectrum at 150 Torr. b) Voigt modeling of the ammonia spectrum at 52.1 Torr.

The results of this modeling are in Fig 4.5. The ammonia spectra had pressure broadening FWHM of 1352 MHz, 1109 MHz and 502 MHz for the 248 Torr, 150 Torr and 52.1 Torr spectra respectively. The pressure broadening FWHM correspond to cell pressures of 157 Torr, 129 Torr, and 56 Torr respectively. The gauge reading and the pressure broadening calculations have good agreement between their values. This is even stronger evidence that the peaks observed are a real signal. The pressure broadening of the 248 Torr spectrum is significantly lower than what is expected (2000 MHz). This could be because the standard deviation of the frequency of each comb tooth is 400 MHz, which is 4 times larger that the standard deviations of the 150 and 52.1 Torr spectra. The ammonia spectra shown in this chapter promising first steps to collecting a full dual comb spectrum with mismatched combs.

CHAPTER 5

SUMMARY AND FUTURE STEPS.

The first part of this work describes a novel EO-comb. This comb has >120 GHz of optical bandwidth, while maintaining a MHz repetition rate. The driving frequencies are digitally tunable to modify the EO-comb to suit the experiment being performed. The construction and implementation of this comb are exceedingly easy, the characterization is non-trivial. The characterization methods described while effective, are an invention on necessity. The EO-comb is too broad for a simple comb CW laser heterodyne and too narrow for a grating spectrometer. A spectrum has been recorded but has not been included here. However, I feel like there is a beauty in the variety of optical methods used to quantify this novel comb. The EO-comb described in the first section does improve upon EO-combs with similar repetition rates, having a greatly improved bandwidth with increased tunability.

The second part of this work is the development and implementation of dual comb spectroscopy using the EO-comb. The main difficulties for performing this measurement are the stabilization of the oscillator. Which have been described here, but the frustration in optimizing these controls cannot be fully quantified. However, the experiment described in this work was able to quantify a singular ammonia transition in the gas phase. The resolution was great enough to perform preliminary line-shape analysis to confirm the detection of ammonia. The next step is to use the full bandwidth of the EO-comb to quantify multiple transitions of ammonia.

The Yb fiber oscillator described in this work is a duplicate of other lasers in lab. This was to validate and learn about collecting dual comb spectra with mismatched combs, while not delaying progress on other experiments. When the dual comb data collection is fully validated, this detection/spectroscopy method can be applied to the transient absorption and 2D experiments that are being developed. The most exciting, in my opinion, is the opportunity to

observe the Berry/geometric phase as a molecule around a conical intersection. The ultrafast nature of the oscillator described in this work is unfortunately not utilized, but will be taken advantage of in the other experiments in the Reber Lab. It is important to note that since both the transient absorption and 2D experiments are cavity enhanced, the repetition rate and f_0 stabilization are already well characterized and implemented.

APPENDIX A

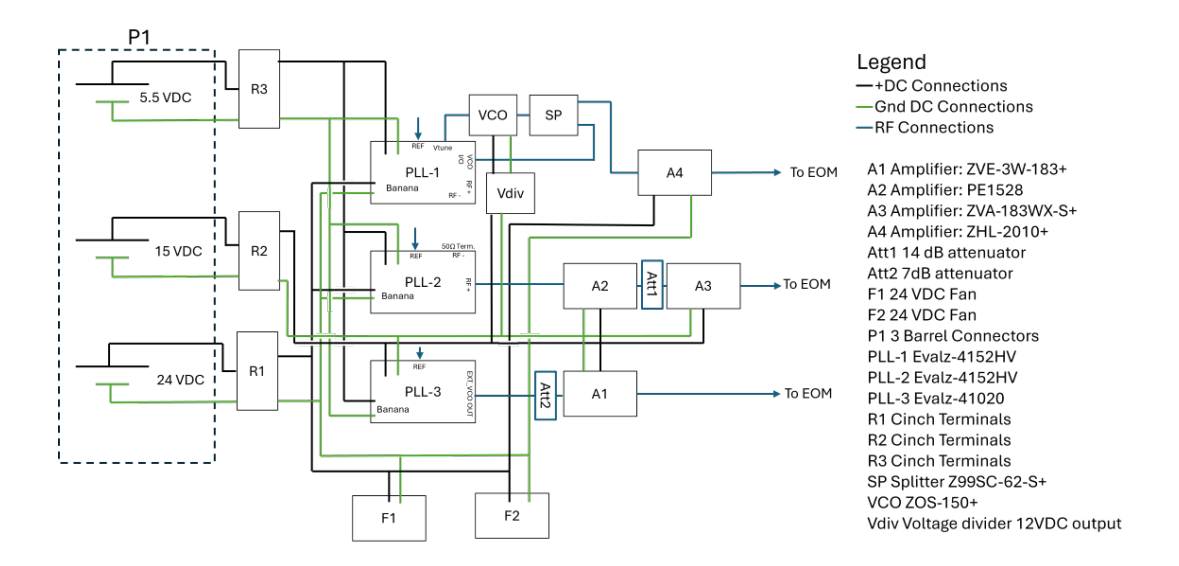


Figure A.I: Circuit Diagram of the PLL Box. The ports that are used for each PLL evaluation board are labeled.

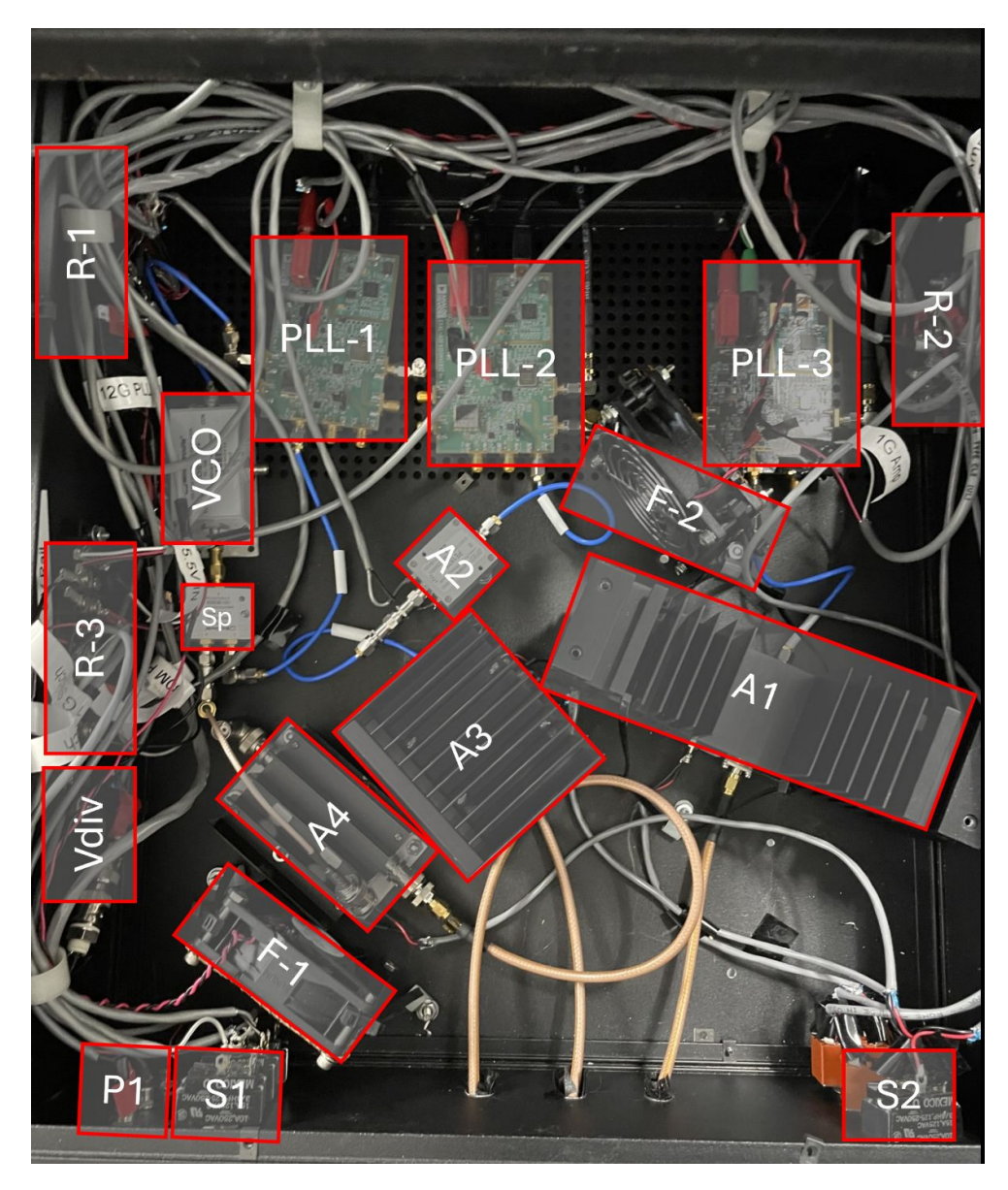


Figure A.2: Labeled Picture of the PLL Box.

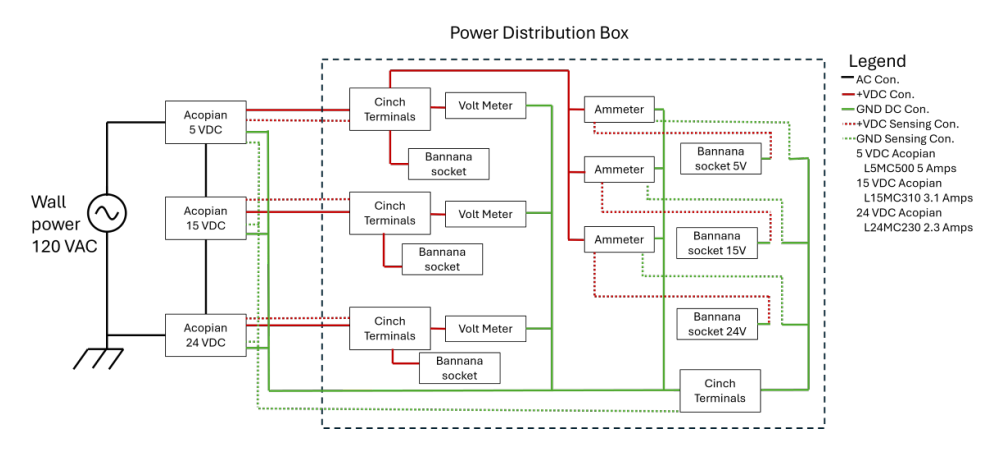


Figure A.3: Circuit diagram of the Power distribution box.

A.1 LabVIEW Programs

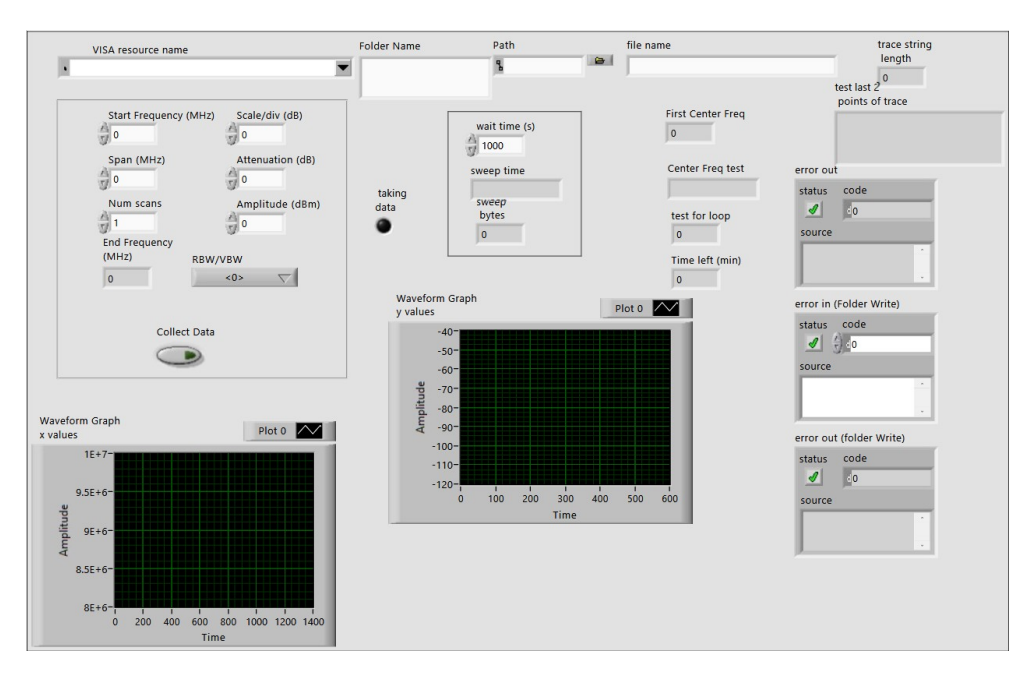


Figure A.4: This is the front panel for the RF spectra auto-collection program.

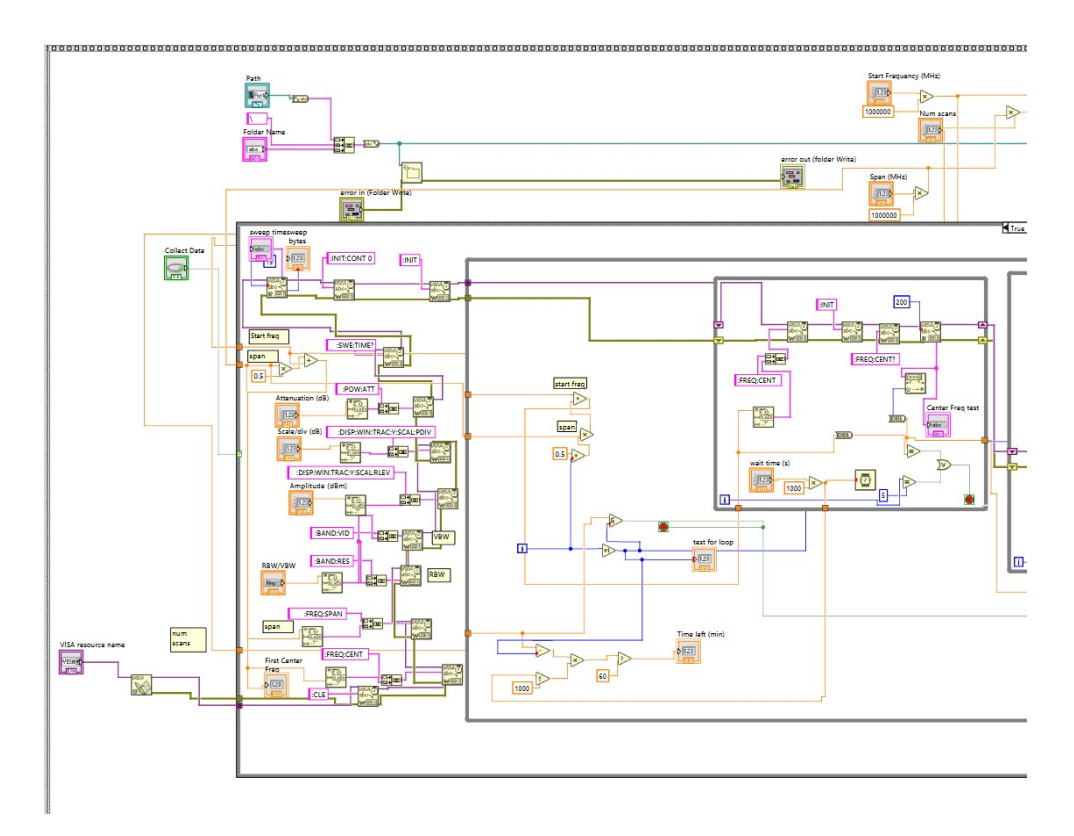


Figure A.5: This is the first part of the block diagram for the RF spectra auto-collection program.

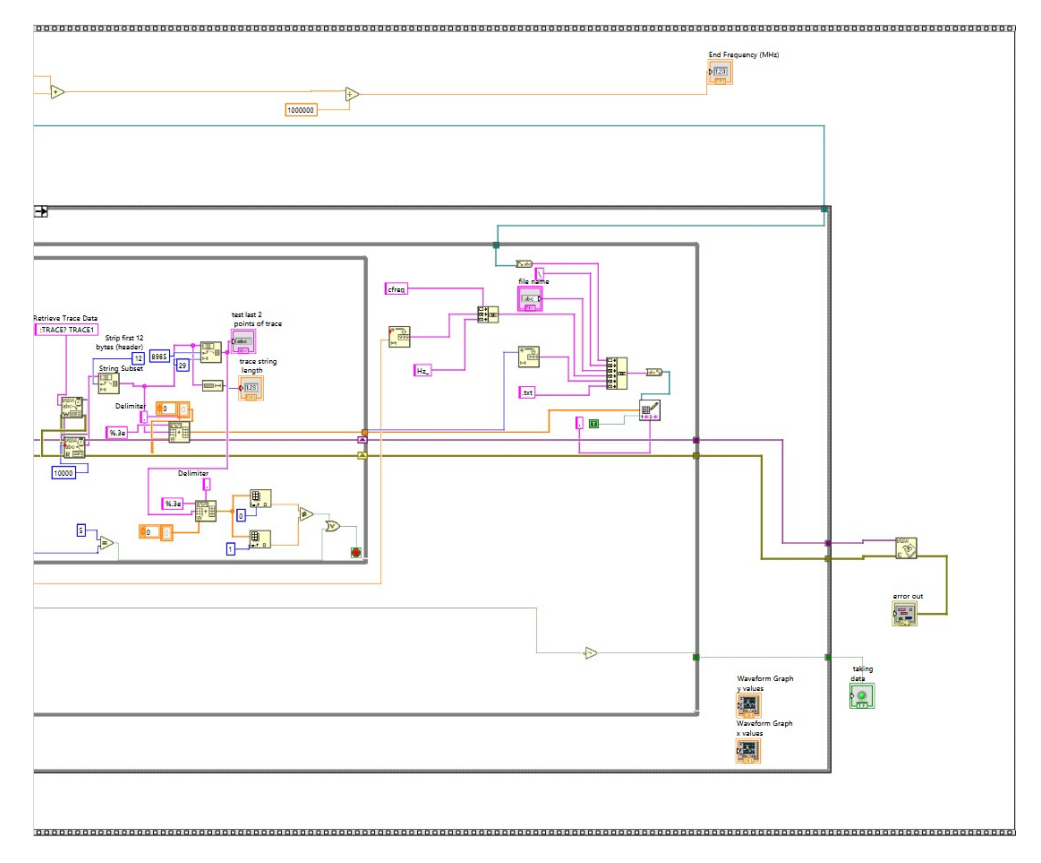


Figure A.6: This is the second part of the block diagram for the RF spectra auto-collection program.

A.2 MATLAB Programs

A.2.1 f_0 Bandwidth Code

```
% range of f0 beat
clear;
import_ui = true;
if import_ui == true
    [file,location] = uigetfile('*.csv');
    trace_ui = readmatrix(file);
    disp(file)
end
data_hold = trace_ui;
%% getting the range by setting a threshold
mhz = data_hold(:,1)./10^6;
dBm = data_hold(:,3);
std_dBm = std(dBm);
thresh_mean = mean(dBm);
thresh_val = 1*std_dBm+thresh_mean;
thresh_plot = zeros(length(mhz),1)+thresh_val;
idx_range = find(dBm >= thresh_val);
mhz_range = mhz(idx_range);
dBm_range = dBm(idx_range);
range_val = max(mhz_range)-min(mhz_range);
disp('Range')
disp(range_val)
figure
    hold on
    plot(mhz, dBm, 'o')
```

```
plot(mhz_range, dBm_range, 'k')
plot(mhz, thresh_plot)
hold off
```

A.2.2 RedPitya 4 Channel Data Acquisition

```
% Script from redpita to collect RF waveform
%% Define Red Pitaya as TCP/IP object
clear all
close all
clc
IP = '192.168.178.111';
                                        % Input IP of your Red Pitaya...
port = 5000;
RP = tcpclient(IP, port);
%% Constants for the data aquisition
dec = 1;
    % decimation of the data, how many points to
    % skip in record needs to be
    % power of 2
trigger = false;
sample_rate = 125*10^6;
    sara = sample_rate/dec;
    ts = 1/sara;
mem_depth = 16*10^3; % max value is 16k
% 'HV' vs 'LV' for each channel
c1_V = 'HV';
c2_V = 'HV';
c3_V = 'HV';
c4_V = 'HV';
% selecting which channels to collect
c1_bool = true;
c2_bool = true;
c3_bool = false;
c4_bool = false;
pause_time = mem_depth/(sample_rate/dec);
```

```
%% Open connection with your Red Pitaya
RP.ByteOrder = 'big-endian';
configureTerminator(RP,'CR/LF');
flush(RP);
% Reset Acquisition
writeline(RP,'ACQ:RST');
%% ACQUISITION
% Set decimation value (sampling rate) in respect to your
% acquired signal frequency
dec_str = append('ACQ:DEC ', num2str(dec));
writeline(RP, dec_str);
buffer_size = writeread(RP, 'ACQ:BUF:SIZE?');
disp(buffer_size)
% setting the HV vs LV for each channel
c1_V_str = append('ACQ:SOUR1:GAIN', c1_V);
c2_V_str = append('ACQ:SOUR2:GAIN', c2_V);
c3_V_str = append('ACQ:SOUR3:GAIN', c3_V);
c4_V_str = append('ACQ:SOUR4:GAIN', c4_V);
writeline(RP, c1_V_str);
writeline(RP, c2_V_str);
writeline(RP, c3_V_str);
writeline(RP, c4_V_str);
% ACQ:SOUR*:COUP AC is the coupling command for each channel * is the
% channel number
% ACQ:DATA:Units <units> sets the output units, options are 'V' or 'Raw"
% Set trigger delay to 0 samples
% O samples delay sets trigger to center of the buffer
% Signal on your graph will have trigger in the center (symmetrical)
\% Samples from left to the center are samples before the trigger
% Samples from center to the right are samples after the trigger
```

```
writeline(RP,'ACQ:TRig:DLY 0');
% for SIGNALlab device there is a possiblity
% to set the trigger threshold
% writeline(RP,'ACQ:TRig:EXT:LEV 1')
%% Start & Trigg
% Trigger source setting must be after ACQ:START
% Set trigger to source 1 positive edge
writeline(RP,'ACQ:START');
% After acquisition is started some time delay
% is needed in order to acquire fresh samples in to buffer
pause(pause_time);
% Here we have used time delay of one second but you
% can calculate the exact value taking in to account buffer
% length and sampling rate
if trigger == true
    % writeline(RP,'ACQ:TRig NOW');
    % % Wait for trigger
    % % Until trigger is true wait with acquiring
    % % Be aware of while loop if trigger is not achieved
    % % Ctrl+C will stop code execution in MATLAB
    %
    % while 1
          trig_rsp = writeread(RP, 'ACQ:TRig:STAT?')
    %
          if strcmp('TD', trig_rsp(1:2)) % Read only TD
    %
              break;
    %
          end
    % end
    %%! OS 2.00 or higher only !%%
    % wait for fill adc buffer
    while 1
        fill_state = writeread(RP,'ACQ:TRig:FILL?')
        if strcmp('1', fill_state(1:1))
            break:
```

```
end
    \quad \text{end} \quad
end
% Read data from buffer
if c1_bool == true
    signal_str = writeread(RP,'ACQ:SOUR1:DATA?');
end
if c2_bool == true
    signal_str_2 = writeread(RP,'ACQ:SOUR2:DATA?');
end
if c3_bool == true
    signal_str_3 = writeread(RP, 'ACQ:SOUR3:DATA?');
end
if c4_bool == true
    signal_str_4 = writeread(RP, 'ACQ:SOUR4:DATA?');
end
% Convert values to numbers.
% The first character in string is "{"
% and the last 3 are 2 spaces and "\".
if c1_bool == true
    signal_num = str2num(signal_str (1, 2:length(signal_str) - 3));
end
if c2_bool == true
    signal_num_2 = str2num(signal_str_2(1, 2:length(signal_str_2) - 3));
end
if c3_bool == true
    signal_num_3 = str2num(signal_str_3(1, 2:length(signal_str_3) - 3));
end
if c4_bool == true
    signal_num_4 = str2num(signal_str_4(1, 2:length(signal_str_4) - 3));
end
time = 0:ts:(buffer_size-1)*ts;
    time = transpose(time);
plot(time, signal_num)
hold on
```

```
plot(time, signal_num_2,'r')
grid on
ylabel('Voltage / V')
xlabel('Time (s)')
savedata = [time, transpose(signal_num), transpose(signal_num_2)];
clear RP;
```

A.2.3 RedPitya DMA Data Acquisition

```
% Redpitya DMA collection
%% Define Red Pitaya as TCP/IP object
clear all
close all
% clc
IP = '172.19.192.137';
                                    % Input IP of your Red Pitaya...
port = 5000;
RP = tcpclient(IP, port);
%% Defining the parameters for the data collection
dec = 1;
sample_rate = 125*10^6; %Sa/s
    sara = sample_rate/dec;
   ts = 1/sara;
trig_lvl = 0.2;
% 'HV' vs 'LV' for each channel
c1_V = 'LV';
c2_V = 'LV';
% selecting which channels to collect
c1_bool = true;
c2_bool = true;
pause_time = ram_allo/(sample_rate/dec);
% size in samples 16-Bit
```

```
% ((1024 * 1024 * 128) / 2)
DATA\_SIZE = 524288;
%% for 128 MB %%
READ_DATA_SIZE = 524288; % (1024 * 256)
%% for 128 MB %%
% max 2097152
%% Open connection with your Red Pitaya
RP.ByteOrder = "big-endian";
 configureTerminator(RP, "CR/LF");
 flush(RP);
 % Reset Acquisition
 writeline(RP,'ACQ:RST');
% Get Memory region
 start_address = str2num(writeread(RP, 'ACQ:AXI:START?'));
 size = str2num(writeread(RP,'ACQ:AXI:SIZE?'));
 start_address2 = round(start_address + size/2);
 fprintf('Reserved memory Start: %d Size: %d\n', start_address, size)
% Set decimation
 writeline(RP,append('ACQ:AXI:DEC ', num2str(dec)));
% Set units
writeline(RP,'ACQ:AXI:DATA:UNITS VOLTS');
 % set gain for channels
 writeline( RP, append('ACQ:SOUR1:GAIN ', c1_V));
 writeline( RP, append('ACQ:SOUR2:GAIN ', c2_V));
 % Set trigger delay for both channels
 writeline(RP,append('ACQ:AXI:SOUR1:Trig:Dly ', num2str(DATA_SIZE)));
 writeline(RP,append('ACQ:AXI:SOUR2:Trig:Dly ', num2str(DATA_SIZE)));
 \% Set-up the Channel 1 and channel 2 buffers to each work with half the available me
 writeline(RP, append('ACQ:AXI:SOUR1:SET:Buffer ', ...
```

```
num2str(start_address), ',', num2str(size/2)));
 writeline(RP, append('ACQ:AXI:SOUR2:SET:Buffer ', ...
    num2str(start_address2), ',', num2str(size/2)));
 % Enable DMA
 writeline(RP, 'ACQ:AXI:SOUR1:ENable ON');
 writeline(RP, 'ACQ:AXI:SOUR2:ENable ON');
 fprintf('Enable CHA and CHB\n');
 % Specify the acquisition trigger
 writeline(RP, append('ACQ:TRig:LEV ', num2str(trig_lvl)));
 %% ACQUISITION
 writeline(RP,'ACQ:START');
 writeline(RP,'ACQ:TRig CH1_PE');
%% Wait for trigger
%
    while 1
%
        trig_rsp = writeread(RP, 'ACQ:TRig:STAT?');
%
        if strcmp('TD',trig_rsp(1:2))
%
            fprintf('Triggered\n');
%
            pause(1);
%
            break;
%
        end
%
    end
 % wait for fill adc buffer
 while 1
     fill_state = writeread(RP,'ACQ:AXI:SOUR1:TRIG:FILL?');
     if strcmp('1', fill_state(1:1))
         fprintf('DMA buffer full\n');
         break;
     end
 end
 % Stop Acquisition
```

```
writeline(RP,'ACQ:STOP');
% Get write pointer at trigger location
posChA = writeread(RP, 'ACQ:AXI:SOUR1:Trig:Pos?');
posChB = writeread(RP, 'ACQ:AXI:SOUR2:Trig:Pos?');
%% Read & plot
signal_str = writeread(RP, append('ACQ:AXI:SOUR1:DATA:Start:N? ', ...
   posChA, ',', num2str(READ_DATA_SIZE)));
signal_str2 = writeread(RP, append('ACQ:AXI:SOUR2:DATA:Start:N?', ...
  posChB, ',', num2str(READ_DATA_SIZE)));
signal_num = str2num(signal_str(1, 2:length(signal_str) - 3));
signal_num2 = str2num(signal_str2(1, 2:length(signal_str2) - 3));
x = linspace(1, READ_DATA_SIZE, READ_DATA_SIZE, READ_DATA_SIZE, READ_DATA_SIZE);
tiledlayout(4,1)
length(x);
length(signal_num);
length(signal_num2);
% CH1 plot
nexttile
plot(x, signal_num)
title('CH1 data')
grid on
% CH2 plot
nexttile
plot(x, signal_num2)
title('CH2 data')
time = 0:ts:((length(x)-1)*ts);
savedata = [transpose(time), transpose(signal_num), transpose(signal_num2)];
%% Close connection with Red Pitaya
writeline(RP, 'ACQ:AXI:SOUR1:ENable OFF');
```

```
writeline(RP, 'ACQ:AXI:SOUR2:ENable OFF');
fprintf('Releasing resources\n');
clear RP;
```

A.2.4 Fourier Transform and Peak Picking Program

```
% FFT of 4 channel data
% clear;
import_ui = 0;
selected_idx = 24895;
if import_ui == true
    [file,location] = uigetfile('*.txt');
    trace_ui = readmatrix(file);
    disp(file)
end
%% Performing standard FFT no chopping
% data_hold = trace_ui;
% time = data_hold(:,1);
% ch1 = data_hold(:,2);
% ch2 = data_hold(:,3);
% ch2 = ch2-mean(ch2);
% ch3 = data_hold(:,4);
% ch3 = ch3-mean(ch3);
% ch4 = data_hold(:,5);
% ch4 = ch4-mean(ch4);
% n_pad = 2^15;
% ts = time(2) - time(1);
% sara = 1/ts;
% L1 = n_pad;
% f1 = sara*(0:(L1/2))/L1;
                             % freq domain
% freqstep = f1(2)-f1(1);
\% freq_idx = find(f1>=20*10^6 & f1<=60*10^6);
```

```
%
% Y1 = fft(ch2, n_pad);
% P2_1 = abs(Y1/L1);
% P1_1 = P2_1(1:L1/2+1);
% P1_1(2:end-1) = 2*P1_1(2:end-1);
% P1_1rms = P1_1*(1/(1*sqrt(2)));
\% t1_dBm = 10*log10((P1_1rms.^2/50)*1000);
%
% Y2 = fft(ch3, n_pad);
% P2_2 = abs(Y2/L1);
% P1_2 = P2_2(1:L1/2+1);
% P1_2(2:end-1) = 2*P1_2(2:end-1);
% P1_2rms = P1_2*(1/(1*sqrt(2)));
\% t2_dBm = 10*log10((P1_2rms.^2/50)*1000);
%
% Y3 = fft(ch4, n_pad);
% P2_3 = abs(Y3/L1);
% P1_3 = P2_3(1:L1/2+1);
% P1_3(2:end-1) = 2*P1_3(2:end-1);
% P1_3rms = P1_3*(1/(1*sqrt(2)));
\% t3_dBm = 10*log10((P1_3rms.^2/50)*1000);
%
% figure
%
      hold on
%
      % plot(f1/10^6, t1_dBm)
%
%
      plot(f1/10^6, t2_dBm)
%
      plot(f1/10^6, t3_dBm)
%
      hold off
%
      title('full trace')
      ylim([-120 -50])
% % %
          % xlim([0 1])
%% getting peaks from the FFT so they can be exported
% trace_15 = readmatrix('3-21_DC testdata\trace_16.txt');
% time = trace_15(:,1);
% ch3 = trace_{15}(:,4);
% ch4 = trace_15(:,5);
```

```
% data_hold = trace_ui;
% time = data_hold(:,1);
% ch1 = data_hold(:,2);
% ch2 = data_hold(:,3);
% ch2 = ch2-mean(ch2);
% ch3 = data_hold(:,4);
% ch3 = ch3-mean(ch3);
% ch4 = data_hold(:,5);
% ch4 = ch4-mean(ch4);
%
% pk_pick_sel = false;
% freq_low = 12; % MHz
% freq_hi = 19; %MHz
%
% n_pad = 31250; %2^14
\% sara = (125*10^6)/2;
% ts = 1/sara;
%
%
% L1 = n_pad;
% f1 = sara*(0:(L1/2))/L1;
                             % freq domain
% f_mhz = f1/10^6;
\% freqstep = f1(2)-f1(1);
\% freq_idx = find(f1>=20*10^6 & f1<=60*10^6);
%
% Y3 = fft(ch3, n_pad);
% P2_3 = abs(Y3/L1);
% P1_3 = P2_3(1:L1/2+1);
% P1_3(2:end-1) = 2*P1_3(2:end-1);
% P1_3rms = P1_3*(1/(1*sqrt(2)));
% t3_mw = (P1_3rms.^2/50);
\% t3_dBm = 10*log10((P1_3rms.^2/50)*1000);
%
% Y4 = fft(ch4, n_pad);
\% P2_4 = abs(Y4/L1);
% P1_4 = P2_4(1:L1/2+1);
% P1_4(2:end-1) = 2*P1_4(2:end-1);
\% P1_4rms = P1_4*(1/(1*sqrt(2)));
```

```
\% t4_mw = (P1_4rms.^2/50);
\% t4_dBm = 10*log10((P1_4rms.^2/50)*1000);
%
%
\% \text{ pk_sep} = 95; \%0.15/(f_mhz(2)-f_mhz(1)); \% \text{ MHz}
\% pk_thresh = 0.25*10^-5;
%
% if pk_pick_sel == true
%
      sel_idx = find(f_mhz >= freq_low & f_mhz <= freq_hi);</pre>
%
      f_sel = f_mhz(sel_idx);
%
          f_sel = transpose(f_sel);
%
      ch3_sel = P1_3rms(sel_idx);
%
      ch4_sel = P1_4rms(sel_idx);
%
%
      % [ch3_pks, ch3_locs] = findpeaks(ch3_sel, f_sel, ...
      %
             'MinPeakDistance', pk_sep, ...
%
             'MinPeakHeight', pk_thresh);
%
      [ch4_pks, ch4_idx] = findpeaks(ch4_sel, 'MinPeakDistance', pk_sep, ...
%
           'MinPeakHeight', pk_thresh);
%
      ch4_locs = f_sel(ch4_idx);
%
      ch3_pks = ch3_sel(ch4_idx);
%
%
      figure
%
          hold on
%
          plot(f_sel, ch4_sel, 'k')
%
          plot(f_sel, ch3_sel)
%
          plot(ch4_locs, ch3_pks, 'o')
%
          plot(ch4_locs, ch4_pks, 'x')
%
          hold off
%
          % xlim([12 19])
% else
%
      [ch4_pks, ch4_idx] = findpeaks(P1_4rms, 'MinPeakDistance', pk_sep, ...
%
           'MinPeakHeight', pk_thresh);
%
      ch4_locs = f_mhz(ch4_idx);
%
      ch3_pks = P1_3rms(ch4_idx);
%
      % I need to redo this method using the delta frep to enforce the delta
%
      % frep spacing
%
%
      figure
```

```
%
          hold on
%
          plot(f_mhz, P1_4rms, 'k')
%
          plot(f_mhz, P1_3rms)
%
          plot(ch4_locs, ch3_pks, 'o')
%
          plot(ch4_locs, ch4_pks, 'x')
%
          hold off
%
          % xlim([0 3])
% end
%
% spectra_pkpick = [transpose(ch4_locs), ch3_pks, ch4_pks];
%
% figure
%
      hold on
%
      plot(ch4_locs, ch3_pks./ch4_pks)
%
      hold off
%
      title('Absorbance')
%% shifting the DC spectra to average together
% import_sel = true;
%
% if import_sel == true
%
      t_44 = readmatrix('3-20_DC_NDandNH3\trace_44.txt');
%
      t_45 = readmatrix('3-20_DC_NDandNH3\trace_45.txt');
%
      t_46 = readmatrix('3-20_DC_NDandNH3\trace_46.txt');
%
      t_47 = readmatrix('3-20_DC_NDandNH3\trace_47.txt');
%
      t_49 = readmatrix('3-20_DC_NDandNH3\trace_49.txt');
%
      t_50 = readmatrix('3-20_DC_NDandNH3\trace_50.txt');
% end
%
% time = t_44(:,1);
% f0_freqs = [28.5947, 28.759, 28.4963, 28.3644, 28.2857, 28.0006];
\% f0_shifts = [0, (28.6942-28.6589), (28.6939-28.6803), ...
%
     (28.3942-28.445), (28.4929-28.4865), 0];
% n_{pad} = 2^{15}; %6250
%
% ts = time(2)-time(1);
% sara = 1/ts;
```

```
%
% L1 = n_pad;
% f1 = sara*(0:(L1/2))/L1;
                            % freq domain
\% freqstep = f1(2)-f1(1);
\% freq_idx = find(f1>=20*10^6 & f1<=60*10^6);
%
% Y44 = fft(t_44(:,5), n_pad);
% P2_44 = abs(Y44/L1);
% P1_44 = P2_44(1:L1/2+1);
% P1_44(2:end-1) = 2*P1_44(2:end-1);
% P1_44rms = P1_44*(1/(1*sqrt(2)));
\% % t1_dBm = 10*log10((P1_1rms.^2/50)*1000);
%
% Y45 = fft(t_45(:,5), n_pad);
% P2_{45} = abs(Y45/L1);
% P1_45 = P2_45(1:L1/2+1);
% P1_45(2:end-1) = 2*P1_45(2:end-1);
% P1_45rms = P1_45*(1/(1*sqrt(2)));
%
% Y46 = fft(t_46(:,5), n_pad);
% P2_46 = abs(Y46/L1);
% P1_46 = P2_46(1:L1/2+1);
% P1_46(2:end-1) = 2*P1_46(2:end-1);
% P1_46rms = P1_46*(1/(1*sqrt(2)));
%
% Y47 = fft(t_47(:,5), n_pad);
% P2_47 = abs(Y47/L1);
% P1_47 = P2_47(1:L1/2+1);
% P1_47(2:end-1) = 2*P1_47(2:end-1);
% P1_47rms = P1_47*(1/(1*sqrt(2)));
%
% Y49 = fft(t_49(:,5), n_pad);
% P2_49 = abs(Y49/L1);
% P1_49 = P2_49(1:L1/2+1);
% P1_49(2:end-1) = 2*P1_49(2:end-1);
% P1_49rms = P1_49*(1/(1*sqrt(2)));
%
% Y50 = fft(t_50(:,5), n_pad);
% P2_{50} = abs(Y50/L1);
```

```
% P1_50 = P2_50(1:L1/2+1);
% P1_50(2:end-1) = 2*P1_50(2:end-1);
% P1_50rms = P1_50*(1/(1*sqrt(2)));
%
% % avg_rms = (P1_44rms+P1_45rms+P1_46rms)./3;
%
% figure
%
       hold on
%
       plot(f1/10^6, P1_44rms)
       \% plot((f1/10^6)+f0_shifts(2), P1_45rms)
%
%
       % plot((f1/10<sup>6</sup>)+f0_shifts(3), P1_46rms)
%
       % plot((f1/10^6)+f0_shifts(4), P1_47rms)
%
       % plot((f1/10<sup>6</sup>)+f0_shifts(5), P1_49rms)
%
       plot((f1/10^6)+f0_shifts(1), P1_50rms)
%
       % plot(f1/10^6, avg_rms)
%
       hold off
%
%
% f_mhz = f1./10^6;
%
% f_44 = f_mhz + f_shifts(1);
% f_{45} = f_{mhz+f0_{shifts}(2)};
% f_{46} = f_{mhz+f0_shifts(3)};
% f_47 = f_mhz + f_shifts(4);
% f_49 = f_mhz + f_shifts(5);
% f_50 = f_mhz + f_shifts(6);
%
\% \text{ sp}_{44} = \text{spline}(f_{44}, P1_{44rms}, f_{mhz});
\% \text{ sp}_{45} = \text{spline}(f_{45}, P1_{45}, f_{mhz});
% sp_46 = spline(f_46, P1_46rms, f_mhz);
\% \text{ sp}_47 = \text{spline}(f_47, P1_47\text{rms}, f_mhz);
\% \text{ sp}_{49} = \text{spline}(f_{49}, P1_{49} \text{rms}, f_{mhz});
\% \text{ sp}_{50} = \text{spline}(f_{50}, P1_{50}, f_{mhz});
%
\% \text{ rms}_{avg} = (sp_44+sp_45+sp_46+sp_47+sp_49+sp_50)./6;
%
% % figure
% %
         hold on
% %
         plot(f_mhz, sp_44)
```

```
% %
        % plot(f_mhz, sp_45)
% %
        % plot(f_mhz, sp_46)
% %
        % plot(f_mhz, sp_47)
% %
        % plot(f_mhz, sp_49)
% %
        % plot(f_mhz, sp_50)
% %
        plot(f_mhz, rms_avg)
% %
       hold off
% %
       ylim([0 5*10^-4])
%% using delta frep to select out DC signal
% and peak picking for DCS
data_hold = trace_ui;
time = data_hold(:,1);
ch1 = data_hold(:,2);
ch2 = data_hold(:,3);
ch2 = ch2-mean(ch2);
ch3 = data_hold(:,4);
ch3 = ch3-mean(ch3);
ch4 = data_hold(:,5);
ch4 = ch4-mean(ch4);
delta_f = 0.25; %MHz
sara = (125*10^6);
ts = 1/sara;
pts_interfer = (1/(delta_f*10^6))*sara;
num_interfer = 100;
n_pad = pts_interfer*num_interfer; %2^14
L1 = n_pad;
f1 = sara*(0:(L1/2))/L1; % freq domain
f_mhz = f1/10^6;
freqstep = f1(2)-f1(1);
freq_idx = find(f1>=20*10^6 \& f1<=60*10^6);
```

```
% f0 beat
Y2 = fft(ch2, n_pad);
P2_2 = abs(Y2/L1);
P1_2 = P2_2(1:L1/2+1);
P1_2(2:end-1) = 2*P1_2(2:end-1);
P1_2rms = P1_2*(1/(1*sqrt(2)));
t2_dBm = 10*log10((P1_2rms.^2/50)*1000);
% [ch2_pks, ch2_idx] = findpeaks(P1_2rms, 'MinPeakHeight', (3*10^-4));
%
      ch2_locs = f_mhz(ch2_idx);
% signal arm
Y3 = fft(ch3, n_pad);
P2_3 = abs(Y3/L1);
P1_3 = P2_3(1:L1/2+1);
P1_3(2:end-1) = 2*P1_3(2:end-1);
P1_3rms = P1_3*(1/(1*sqrt(2)));
t3_dBm = 10*log10((P1_3rms.^2/50)*1000);
% background arm
Y4 = fft(ch4, n_pad);
P2_4 = abs(Y4/L1);
P1_4 = P2_4(1:L1/2+1);
P1_4(2:end-1) = 2*P1_4(2:end-1);
P1_4rms = P1_4*(1/(1*sqrt(2)));
t4_dBm = 10*log10((P1_4rms.^2/50)*1000);
figure
    hold on
    plot(f_mhz, P1_2rms)
    % plot(ch2_locs, ch2_pks, 'o')
    hold off
    title('Peak pick of f0')
%
% figure
%
          hold on
%
          plot(f_mhz, P1_4rms, 'k')
%
          plot(f_mhz, P1_3rms)
%
          hold off
```

```
%
         title('FFT of data')
harmonic = 1; % 1g is 14th
pts_spacing = ((delta_f*10^6)/freqstep)*harmonic+1;
pts_spread = 40;
n_fft = length(P1_4rms);
pts_start = mod(selected_idx, pts_spacing);
centerpt_array = (pts_start):pts_spacing:(n_fft);
% ch4_data_array = zeros(length(centerpt_array), 3);
ch3_data_array = zeros(length(centerpt_array), 4);
for k = 1:length(centerpt_array)
    loop_idxst = centerpt_array(k)-pts_spread;
    loop_idxen = centerpt_array(k)+pts_spread;
        if loop_idxen > n_fft
            loop_idxen = n_fft;
        end
        if loop_idxst < 1</pre>
            loop_idxst = 1;
        end
    loop_data_ch3 = P1_3rms(loop_idxst:loop_idxen);
    [loop_max3, loop_idx3] = max(loop_data_ch3);
    loop_data_idx3 = loop_idx3+loop_idxst-1;
    ch3_data_array(k,:) = [f_mhz(loop_data_idx3), loop_max3, ...
        P1_4rms(loop_data_idx3), loop_data_idx3];
    % ch4_data_array(k,:) = [f_mhz(loop_data_idx3), ...
        P1_4rms(loop_data_idx3), loop_data_idx3];
end
% for a figure performing the inverse fft
ifft_low = 29.5; %mhz
ifft_high = 35; % mhz
idx_filter = find(f_mhz <= ifft_low | f_mhz >= ifft_high);
fft_filtered = P1_3rms;
fft_filtered(idx_filter) = 0;
fft_filtered = transpose(fft_filtered);
```

```
Yi2_filtered = [fft_filtered(1) fft_filtered(2:end)/2 ...
    fliplr(conj(fft_filtered(2:end)))/2];
ch3_filter = ifft(Yi2_filtered);
time_ifft = 0:ts:(ts*(length(ch3_filter)-1));
figure
    hold on
    plot(time_ifft-(5*10^-5), ch3_filter)
    hold off
    xlabel('Time (s)')
    ylabel('Amplitude (V)')
    xlim([0 1.5*10^-4])
% figure
%
      hold on
%
      plot(P1_4rms)
%
      plot(ch3_data_array(:,4), ch3_data_array(:,3), 'o')
%
      hold off
%
      title('CH4 selecting idx of a real peak')
% figure
%
      hold on
%
      plot( P1_3rms)
%
      plot(ch3_data_array(:,4), ch3_data_array(:,2), 'o')
%
      hold off
%
      title('CH3 selecting idx of a real peak')
figure
    hold on
    plot(f_mhz-32.2825, P1_3rms)
    % plot(ch3_data_array(119:138,1)-32.2825, ch3_data_array(119:138,2),
    % plot(ch3_data_array(129,1)-32.2825, ch3_data_array(129,2), 'ko')
    hold off
    xlabel('Relative FFT Frequency (MHz)')
    xlim([-4 4])
    ylabel('Power (V_{rms})')
% figure
%
      hold on
```

```
%
      plot(ch3_data_array(:,1), ch3_data_array(:,2)./ch3_data_array(:,3))
%
      hold off
%
      title('Transmission?')
%% seeing if I can average ffts together
\% t_1 = readmatrix('4-4_testDC\4-4_46.txt');
\% t_2 = readmatrix('4-4_testDC\4-4_47.txt');
\% t_3 = readmatrix('4-4_testDC\4-4_48.txt');
\% t_4 = readmatrix('4-4_testDC\4-4_49.txt');
\% t_5 = readmatrix('4-4_testDC\4-4_50.txt');
\% t_6 = readmatrix('4-4_testDC\4-4_51.txt');
\% t_7 = readmatrix('4-4_testDC\4-4_52.txt');
\% t_8 = readmatrix('4-4_testDC\4-4_53.txt');
\% t_9 = readmatrix('4-4_testDC\4-4_54.txt');
\% t_10 = readmatrix('4-4_testDC\4-4_55.txt');
%
% pk_select = true;
% f0_idx_ident = false;
%
%
% time = t_1(:,1);
% channel_num = 4;
% ch3_t1 = t_1(:,channel_num);
\% ch3_t2 = t_2(:,channel_num);
% ch3_t3 = t_3(:,channel_num);
\% ch3_t4 = t_4(:,channel_num);
\% ch3_t5 = t_5(:,channel_num);
\% ch3_t6 = t_6(:,channel_num);
% ch3_t7 = t_7(:,channel_num);
% ch3_t8 = t_8(:,channel_num);
\% ch3_t9 = t_9(:,channel_num);
% ch3_t10 = t_10(:,channel_num);
%
%
% ch3_t1 = ch3_t1 - mean(ch3_t1);
% ch3_t2 = ch3_t2 - mean(ch3_t2);
% ch3_t3 = ch3_t3 - mean(ch3_t3);
\% ch3_t4 = ch3_t4 - mean(ch3_t4);
```

```
% ch3_t5 = ch3_t5 - mean(ch3_t5);
% ch3_t6 = ch3_t6 - mean(ch3_t6);
% ch3_t7 = ch3_t7 - mean(ch3_t7);
% ch3_t8 = ch3_t8 - mean(ch3_t8);
% ch3_t9 = ch3_t9 - mean(ch3_t9);
% ch3_t10 = ch3_t10 - mean(ch3_t10);
%
\% delta_f = 0.25; \%MHz
\% sara = (125*10^6);
% ts = 1/sara;
% pts_interfer = (1/(delta_f*10^6))*sara;
% num_interfer = 100;
% n_pad = pts_interfer*num_interfer; %2^14
%
% L1 = n_pad;
% f1 = sara*(0:(L1/2))/L1;  % freq domain
% f_mhz = f1/10^6;
\% freqstep = f1(2)-f1(1);
\% freq_idx = find(f1>=20*10^6 & f1<=60*10^6);
%
% Y1 = fft(ch3_t1, n_pad);
% P2_1 = abs(Y1/L1);
% P1_1 = P2_1(1:L1/2+1);
% P1_1(2:end-1) = 2*P1_1(2:end-1);
% P1_1rms = P1_1*(1/(1*sqrt(2)));
\% t1_dBm = 10*log10((P1_1rms.^2/50)*1000);
%
% Y2 = fft(ch3_t2, n_pad);
% P2_2 = abs(Y2/L1);
% P1_2 = P2_2(1:L1/2+1);
% P1_2(2:end-1) = 2*P1_2(2:end-1);
% P1_2rms = P1_2*(1/(1*sqrt(2)));
\% t2_dBm = 10*log10((P1_2rms.^2/50)*1000);
%
% Y3 = fft(ch3_t3, n_pad);
% P2_3 = abs(Y3/L1);
% P1_3 = P2_3(1:L1/2+1);
% P1_3(2:end-1) = 2*P1_3(2:end-1);
% P1_3rms = P1_3*(1/(1*sqrt(2)));
```

```
\% t3_dBm = 10*log10((P1_3rms.^2/50)*1000);
% Y4 = fft(ch3_t4, n_pad);
% P2_4 = abs(Y4/L1);
% P1_4 = P2_4(1:L1/2+1);
% P1_4(2:end-1) = 2*P1_4(2:end-1);
% P1_4rms = P1_4*(1/(1*sqrt(2)));
\% t4_dBm = 10*log10((P1_4rms.^2/50)*1000);
% Y5 = fft(ch3_t5, n_pad);
% P2_5 = abs(Y5/L1);
\% P1_5 = P2_5(1:L1/2+1);
% P1_5(2:end-1) = 2*P1_5(2:end-1);
% P1_5rms = P1_5*(1/(1*sqrt(2)));
\% t5_dBm = 10*log10((P1_5rms.^2/50)*1000);
%
% Y6 = fft(ch3_t6, n_pad);
% P2_6 = abs(Y6/L1);
% P1_6 = P2_6(1:L1/2+1);
% P1_6(2:end-1) = 2*P1_6(2:end-1);
% P1_6rms = P1_6*(1/(1*sqrt(2)));
\% t6_dBm = 10*log10((P1_6rms.^2/50)*1000);
%
% Y7 = fft(ch3_t7, n_pad);
% P2_7 = abs(Y7/L1);
% P1_7 = P2_7(1:L1/2+1);
% P1_7(2:end-1) = 2*P1_7(2:end-1);
% P1_7rms = P1_7*(1/(1*sqrt(2)));
\% t7_dBm = 10*log10((P1_7rms.^2/50)*1000);
% Y8 = fft(ch3_t8, n_pad);
% P2_8 = abs(Y8/L1);
% P1_8 = P2_8(1:L1/2+1);
% P1_8(2:end-1) = 2*P1_8(2:end-1);
% P1_8rms = P1_8*(1/(1*sqrt(2)));
\% t8_dBm = 10*log10((P1_8rms.^2/50)*1000);
%
% Y9 = fft(ch3_t9, n_pad);
% P2_9 = abs(Y9/L1);
```

```
% P1_9 = P2_9(1:L1/2+1);
% P1_9(2:end-1) = 2*P1_9(2:end-1);
% P1_9rms = P1_9*(1/(1*sqrt(2)));
\% t9_dBm = 10*log10((P1_9rms.^2/50)*1000);
%
% Y10 = fft(ch3_t10, n_pad);
% P2_10 = abs(Y10/L1);
% P1_10 = P2_10(1:L1/2+1);
% P1_10(2:end-1) = 2*P1_10(2:end-1);
% P1_10rms = P1_10*(1/(1*sqrt(2)));
\% t10_dBm = 10*log10((P1_10rms.^2/50)*1000);
%
% if f0_idx_ident == true
%
                   figure
%
                               hold on
%
                              plot(P1_10rms)
%
                              hold off
% end
% f0_idx_array = [12960, 12918, 12813, 12717, 12840, ...
            12769, 12758, 12691, 12883, 12797];
% % 7651
% if pk_select == true
%
                   idx_space = 1:1:length(P1_4);
%
                   idx_1 = idx_space-f0_idx_array(1);
%
                   idx_2 = idx_space-f0_idx_array(2);
%
                   idx_3 = idx_space-f0_idx_array(3);
%
                   idx_4 = idx_space-f0_idx_array(4);
%
                   idx_5 = idx_space-f0_idx_array(5);
%
                   idx_6 = idx_space-f0_idx_array(6);
%
                   idx_7 = idx_space-f0_idx_array(7);
%
                   idx_8 = idx_space-f0_idx_array(8);
%
                   idx_9 = idx_space-f0_idx_array(9);
%
                   idx_10 = idx_space-f0_idx_array(10);
%
%
                  min_idx_array = [min(idx_1), min(idx_2), min(idx_3), min(idx_4), m
%
                               min(idx_6), min(idx_7), min(idx_8), min(idx_9), min(idx_10)];
%
                  \max_{i} dx_{array} = [\max(idx_{1}), \max(idx_{2}), \max(idx_{3}), \max(idx_{4}), \max(idx_{1}), \max(idx_{2}), \max(idx_{3}), \max(idx_{4}), \max(idx_{1}), \max(idx_{1}), \max(idx_{2}), \max(idx_{3}), \max(idx_{4}), \max(idx_{4
%
                               max(idx_6), max(idx_7), max(idx_8), max(idx_9), max(idx_10)];
%
                  min_idx = max(min_idx_array);
```

```
%
      max_idx = min(max_idx_array);
%
      idx_plot = min_idx:1:max_idx;
%
%
      sel_1_idx = find(idx_1 >= min_idx & idx_1 <= max_idx);</pre>
%
      sel_2_idx = find(idx_2 >= min_idx & idx_2 <= max_idx);</pre>
%
      sel_3_idx = find(idx_3 >= min_idx & idx_3 <= max_idx);</pre>
%
      sel_4_idx = find(idx_4 >= min_idx & idx_4 <= max_idx);</pre>
%
      sel_5_idx = find(idx_5 >= min_idx & idx_5 <= max_idx);</pre>
%
      sel_6_idx = find(idx_6 >= min_idx & idx_6 <= max_idx);</pre>
%
      sel_7_idx = find(idx_7 >= min_idx & idx_7 <= max_idx);</pre>
%
      sel_8_idx = find(idx_8 >= min_idx & idx_8 <= max_idx);</pre>
%
      sel_9_idx = find(idx_9 >= min_idx & idx_9 <= max_idx);</pre>
%
      sel_10_idx = find(idx_10 >= min_idx & idx_10 <= max_idx);
%
%
      sel_array = [P1_1rms(sel_1_idx), P1_2rms(sel_2_idx), ...
%
          P1_3rms(sel_3_idx), P1_4rms(sel_4_idx), P1_5rms(sel_5_idx),...
%
          P1_6rms(sel_6_idx), P1_7rms(sel_7_idx), ...
%
          P1_8rms(sel_8_idx), P1_9rms(sel_9_idx), P1_10rms(sel_10_idx)];
%
      rms_avg = mean(sel_array,2);
%
      fft_mhz_avg = (idx_plot*freqstep)./10^6;
%
      [pks,locs] = findpeaks(rms_avg, 'MinPeakHeight', 1*10^-5, ...
%
         'MinPeakDistance', 90);
%
      pks_mhz = fft_mhz_avg(locs);
%
      pks_export = [transpose(pks_mhz), pks];
%
%
      % figure
%
      %
            hold on
%
            plot(idx_1, (P1_1rms), 'k')
      %
%
      %
            plot(idx_9, (P1_9rms))
%
      %
            hold off
%
      %
            xlim([50 150])
%
%
      figure
%
          hold on
%
          plot(fft_mhz_avg, (rms_avg))
%
          plot(pks_mhz, pks, 'o')
%
          hold off
% end
```

```
%% FFT of CH1 or frep monitor
% data_hold = trace_ui(:,1:2);
% ch1 = data_hold(:,2);
n_pad = 2^2;
%
% sara = 125*10^6;
% L1 = n_{pad};
% f1 = sara*(0:(L1/2))/L1; % freq domain
% f_mhz = f1/10^6;
% freqstep = f1(2)-f1(1);
\% freq_idx = find(f1>=20*10^6 & f1<=60*10^6);
%
% Y1 = fft(ch1, n_pad);
% P2_1 = abs(Y1/L1);
% P1_1 = P2_1(1:L1/2+1);
% P1_1(2:end-1) = 2*P1_1(2:end-1);
% P1_1rms = P1_1*(1/(1*sqrt(2)));
\% t1_dBm = 10*log10((P1_1rms.^2/50)*1000);
%
% figure
%
      plot(f_mhz, t1_dBm)
%
      xlim([0 1])
```

A.2.5 Voigt Modeling and Fitting Program

```
% performing spectra assignment and stats on 'good data'
clear;
import_42_sel = false;
import_44_0250 = false;
import_44_0125 = false;
import_process_spec = true;

just_fit_gauss = true;
if import_42_sel == true
```

```
% opts = detectImportOptions( '4-2_testDC\matlabdata_61-70_81-90.xlsx',...
%
      'DataRange', 'B6:BY237');
% excel_sheet = readmatrix('4-2_testDC\matlabdata_61-70_81-90.xlsx',...
%
      opts);
% % NH3 data
% t_61 = excel_sheet(:,1:4);
% t_62 = excel_sheet(:,5:8);
% t_63 = excel_sheet(:,9:12);
\% t_64 = excel_sheet(:,13:16);
\% t_65 = excel_sheet(:,17:20);
% t_66 = excel_sheet(:,21:24);
% t_67 = excel_sheet(:,25:28);
% t_68 = excel_sheet(:,29:32);
% t_69 = excel_sheet(:,33:36);
% t_70 = excel_sheet(:,37:40);
% % background data
% t_81 = excel_sheet(:,41:44);
% t_82 = excel_sheet(:,45:48);
% t_83 = excel_sheet(:,49:52);
% t_84 = excel_sheet(:,53:56);
% t_85 = excel_sheet(:,57:60);
% t_86 = excel_sheet(:,61:64);
% t_87 = excel_sheet(:,65:68);
% t_88 = excel_sheet(:,69:72);
% t_90 = excel_sheet(:,73:76);
% nh3_ch3_array = [t_61(:, 2), t_62(:, 2), t_63(:, 2), ...
% t_{64}(:, 2), t_{65}(:, 2), ...
%
      t_{-66}(:, 2), t_{-67}(:, 2), t_{-68}(:, 2), t_{-69}(:, 2),...
% t_70(:, 2)];
% nh3_ch4_array = [t_61(:, 3), t_62(:, 3), t_63(:, 3), ...
%t_64(:, 3), t_65(:, 3), ...
%
      t_{-66}(:, 3), t_{-67}(:, 3), t_{-68}(:, 3), t_{-69}(:, 3), t_{-70}(:, 3)];
% nh3_mhz_array = [t_61(:, 1), t_62(:, 1), t_63(:, 1), ...
% t_64(:, 1), t_65(:, 1), ...
      t_{-66}(:, 1), t_{-67}(:, 1), t_{-68}(:, 1), t_{-69}(:, 1), t_{-70}(:, 1)];
%
%
% na_ch3_array = [t_81(:, 2), t_82(:, 2), t_83(:, 2),...
% t_84(:, 2), t_85(:, 2), ...
      t_{86}(:, 2), t_{87}(:, 2), t_{88}(:, 2), t_{90}(:, 2)];
%
```

```
\% na_ch4_array = [t_81(:, 3), t_82(:, 3), t_83(:, 3), ...
   % t_84(:, 3), t_85(:, 3), ...
          t_86(:, 3), t_87(:, 3), t_88(:, 3), t_90(:, 3)];
    % na_mhz_array = [t_81(:, 1), t_82(:, 1), t_83(:, 1), ...
   %t_84(:, 1), t_85(:, 1), ...
          t_86(:, 1), t_87(:, 1), t_88(:, 1), t_90(:, 1)];
    % harm_num = t_61(:, 4);
end
if import_44_0250 == true
    % opts_1 = detectImportOptions(pkpick_4-4_DCdata_025.xlsx',...
          'Sheet', 1, 'DataRange', 'B6:A0168');
    % excel_1 = readmatrix('4-4_testDC\pkpick_4-4_DCdata_025.xlsx',...
          opts_1);
   % back_025_ch3 = [excel_1(:,2), excel_1(:,6), excel_1(:,10), ...
   % excel_1(:,14), ...
   %
          excel_1(:,18), excel_1(:,22), excel_1(:,26), ...
   % excel_1(:,30), ...
   \% excel_1(:,34), excel_1(:,38)];
   \% back_025_ch4 = [excel_1(:,3), excel_1(:,7), excel_1(:,11), ...
   % excel_1(:,15), ...
          excel_1(:,19), excel_1(:,23), excel_1(:,27), ...
   %
   % excel_1(:,31), ...
        excel_1(:,35), excel_1(:,39)];
   % back_025_harm = excel_1(:,4);
   % opts_2 = detectImportOptions('pkpick_4-4_DCdata_025.xlsx',...
          'Sheet', 2, 'DataRange', 'B6:A0252');
    % excel_2 = readmatrix('4-4_testDC\pkpick_4-4_DCdata_025.xlsx',...
          opts_2);
   % nh3_52_ch3 = [excel_2(:,2), excel_2(:,6), excel_2(:,10), ...
   % excel_2(:,14), ...
   %
          excel_2(:,18), excel_2(:,22), excel_2(:,26), ...
   \% excel_2(:,30), excel_2(:,34), excel_2(:,38)];
   % nh3_52_ch4 = [excel_2(:,3), excel_2(:,7), excel_2(:,11), ...
   % excel_2(:,15), ...
   %
          excel_2(:,19), excel_2(:,23), excel_2(:,27), ...
   \% excel_2(:,31), excel_2(:,35), excel_2(:,39)];
    % \text{ nh3\_52\_mhz} = [\text{excel\_2}(:,1), \text{excel\_2}(:,5), \text{excel\_2}(:,9),...
```

```
% excel_2(:,13), ...
          excel_2(:,17), excel_2(:,21), excel_2(:,25), ...
    %
    \% excel_2(:,29), excel_2(:,33), excel_2(:,37)];
    % nh3_{52}harm = excel_{2}(:,4);
    %
    % opts_3 = detectImportOptions( 'pkpick_4-4_DCdata_025.xlsx',...
          'Sheet', 3, 'DataRange', 'B6:AW250');
    % excel_3 = readmatrix('pkpick_4-4_DCdata_025.xlsx',...
    %
          opts_3);
    % nh3_150_ch3 = [excel_3(:,2), excel_3(:,6), excel_3(:,10), ...
    % excel_3(:,14), ...
    %
          excel_3(:,18), excel_3(:,22), excel_3(:,26), ...
    \% excel_3(:,30), excel_3(:,34), ...
          excel_3(:,38), excel_3(:,42), excel_3(:,46)];
    % \text{ nh3}_{150}\text{ch4} = [\text{excel}_{3}(:,3), \text{excel}_{3}(:,7), \text{excel}_{3}(:,11), \dots
    % excel_3(:,15), ...
          excel_3(:,19), excel_3(:,23), excel_3(:,27), ...
    \% excel_3(:,31), excel_3(:,35), ...
    %
          excel_3(:,39), excel_3(:,43), excel_3(:,47)];
    % \ nh3_150_mhz = [excel_3(:,1), excel_3(:,5), excel_3(:,9), ...
    % excel_3(:,13), ...
          excel_3(:,17), excel_3(:,21), excel_3(:,25), ...
    \% excel_3(:,29), excel_3(:,33), ...
    %
          excel_3(:,37), excel_3(:,41), excel_3(:,45)];
    % nh3_150_harm = excel_3(:,4);
end
if import_44_0125 == true
    % opts_1 = detectImportOptions( 'pkpick_4-4_DCdata_0125.xlsx',...
          'Sheet', 1, 'DataRange', 'B6:Q496');
    % excel_1 = readmatrix('pkpick_4-4_DCdata_0125.xlsx',...
    %
          opts_1);
    % back_0125_ch3 = [excel_1(:,2), excel_1(:,6), excel_1(:,10), ...
    % excel_1(:,14)];
    \% back_0125_ch4 = [excel_1(:,3), excel_1(:,7), excel_1(:,11), ...
    % excel_1(:,15)];
    \% back_0125_harm = excel_1(:,4);
    % opts_2 = detectImportOptions( 'pkpick_4-4_DCdata_0125.xlsx',...
```

```
'Sheet', 2, 'DataRange', 'B6:A0496');
    % excel_2 = readmatrix('pkpick_4-4_DCdata_0125.xlsx',...
    %
          opts_2);
    % nh3_125_ch3 = [excel_2(:,2), excel_2(:,6), excel_2(:,10), ...
    % excel_2(:,14), ...
          excel_2(:,18), excel_2(:,22), excel_2(:,26), ...
    %
    % excel_2(:,30), excel_2(:,34), excel_2(:,38)];
    % nh3_125_ch4 = [excel_2(:,3), excel_2(:,7), excel_2(:,11), ...
    % excel_2(:,15), ...
          excel_2(:,19), excel_2(:,23), excel_2(:,27), ...
    %
    \% excel_2(:,31), excel_2(:,35), excel_2(:,39)];
    % nh3_125_mhz = [excel_2(:,1), excel_2(:,5), excel_2(:,9), ...
    % excel_2(:,13), ...
    %
          excel_2(:,17), excel_2(:,21), excel_2(:,25), ...
    % excel_2(:,29), excel_2(:,33), excel_2(:,37)];
    % nh3_125_harm = excel_2(:,4);
end
if import_process_spec == true
    opts_1 = detectImportOptions( 'collating_NH3spec.xlsx',...
        'Sheet', 1, 'DataRange', 'B6:C168');
    p150 = readmatrix('collating_NH3spec.xlsx',...
        opts_1);
    opts_2 = detectImportOptions( 'collating_NH3spec.xlsx',...
        'Sheet', 1, 'DataRange', 'D6:E160');
    p52 = readmatrix('collating_NH3spec.xlsx',...
        opts_2);
    opts_3 = detectImportOptions( 'collating_NH3spec.xlsx',...
        'Sheet', 1, 'DataRange', 'G6:H237');
    p248 = readmatrix('collating_NH3spec.xlsx',...
        opts_3);
end
% trace order = [MHz, CH3 Vrms, CH4 Vrms, Harmonic]
% making the data arrays
```

```
if just_fit_gauss == false
   % samp_harm = nh3_150_harm;
   % back_harm = back_025_harm;
   % limit_array = [min(samp_harm), min(back_harm); ...
   % max(samp_harm), max(back_harm)];
   % limit_min = max(limit_array(1,:));
   % limit_max = min(limit_array(2,:));
   % limit_idx_samp = find(samp_harm >= limit_min & ...
   % samp_harm <= limit_max);</pre>
   % limit_idx_back = find(back_harm >= limit_min & ...
   % back_harm <= limit_max);</pre>
   %
   % samp_ch3 = nh3_150_ch3(limit_idx_samp,:);
   % samp_ch4 = nh3_150_ch4(limit_idx_samp,:);
   % samp_mhz = nh3_150_mhz(limit_idx_samp,:);
   %
   % back_ch3 = back_025_ch3(limit_idx_back,:);
   % back_ch4 = back_025_ch3(limit_idx_back,:);
   %
   %
   % nh3_ch3_avg = mean(samp_ch3, 2);
   % nh3_ch4_avg = mean(samp_ch4 , 2);
   % nh3_mhz_avg = mean(samp_mhz, 2);
   %
          nh3_mhz_avg = nh3_mhz_avg-min(nh3_mhz_avg);
   %
   %
   % na_ch3_avg = mean(back_ch3, 2);
   % na_ch4_avg = mean(back_ch4, 2);
   %
   % T_nh3 = nh3_ch3_avg ./nh3_ch4_avg;
    % T_na = na_ch3_avg./na_ch4_avg;
   % T_norm = T_nh3./T_na;
   %
   % delta_f = 0.125;
    \% \text{ rep_rate} = 72.403*(72/(72+delta_f));
   % cell_torr = 250; %torr
   % temp = 298; %k
   % m = 17; %amu
    \% p_HW = 4.2074*cell_torr + 12.336;
```

```
\% dopp_c = (((7.2*10^-7)*sqrt(temp/m))*281611.7274)*10^3;
   % nh3_mhz_std = std(samp_mhz, 0, 2)*(rep_rate/0.25);
   % opt_mhz = nh3_mhz_avg*(rep_rate/delta_f);
   % opt_mhz = opt_mhz+(delta_f*limit_min)*(rep_rate/delta_f);
   %
   % % sel_low = 7000;
   % % sel_high = 14000;
   % %
   % % idx_sel = find(opt_mhz>=sel_low & opt_mhz<=sel_high);
   % % mhz_sel = opt_mhz(idx_sel);
   % %
            mhz_sel = mhz_sel-mean(mhz_sel);
   % % T_sel = T_norm(idx_sel);
   % % T_sel = T_sel*-1+1.2;
   % % amp_st = 1;
   % % sigma_st = 1000;
   % % cent_1 = 979;
   % cent_2 = 2304;
   % % gaus_2 = fit(mhz_sel, T_sel, 'gauss2', 'StartPoint', ...
   % %
            [amp_st, cent_1, sigma_st, amp_st, cent_2, sigma_st]);
   % % coeff = coeffvalues(gaus_2);
   \% % fwhm_1 = (coeff(3)/2)*2*sqrt(2*log(2));
   \% \% \text{ fwhm}_2 = (\text{coeff}(6)/2)*2*\text{sqrt}(2*\log(2));
   %
   % figure
   %
          hold on
    %
          % plot(opt_mhz, -1*log(T_norm))
   %
          plot(opt_mhz, T_na)
   %
         plot(opt_mhz, T_nh3)
   %
          % plot(mhz_sel, T_sel, 'o')
   %
          % plot(mhz_sel, gaus_2(mhz_sel))
    %
          hold off
    %
          % xlim([7000 14000])
end
if just_fit_gauss == true
   % adjusting the baselines
   p248(:,2) = p248(:,2)*-1+1.2;
   p150(:,2) = p150(:,2)*-1+2;
   p52(:,2) = p52(:,2)*-1+1.2;
```

```
% poly_fit = fit(p52(:,1), p52(:,2), 'poly3');
\% p52(:,2) = p52(:,2)-poly_fit(p52(:,1));
sel_low = -1000;
sel_high = 3000;
% Fitting gaussians to the data
idx_248 = find(p248(:,1) >= sel_low & p248(:,1) <= sel_high);
mhz_248 = p248(idx_248,1);
T_248 = p248(idx_248, 2);
amp_st = 1;
sigma_st = 1000;
cent_1 = 1000;
gaus_248 = fit(mhz_248, T_248, 'gauss1', 'StartPoint', ...
    [amp_st, cent_1, sigma_st]);
coeff_248 = coeffvalues(gaus_248);
fwhm_248 = (coeff_248(3)/2)*2*sqrt(2*log(2));
idx_150 = find(p150(:,1) >= sel_low & p150(:,1) <= sel_high);
mhz_150 = p150(idx_150,1);
T_150 = p150(idx_150, 2);
amp_st = 1;
sigma_st = 1000;
cent_1 = 1000;
gaus_150 = fit(mhz_150, T_150, 'gauss1', 'StartPoint', ...
    [amp_st, cent_1, sigma_st]);
coeff_150 = coeffvalues(gaus_150);
fwhm_150 = (coeff_150(3)/2)*2*sqrt(2*log(2));
idx_52 = find(p52(:,1) >= sel_low & p52(:,1) <= (sel_high-800));
mhz_52 = p52(idx_52,1);
T_52 = p52(idx_52, 2);
amp_st = 0.2;
sigma_st = 200;
cent_1 = 1000;
gaus_52 = fit(mhz_52, T_52, 'gauss1', 'StartPoint', ...
    [amp_st, cent_1, sigma_st]);
coeff_52 = coeffvalues(gaus_52);
fwhm_52 = (coeff_52(3)/2)*2*sqrt(2*log(2));
```

```
% using polynomal for baseline subtraction
% poly_fit = fit(p52(:,1), p52(:,2), 'poly7');
% figure
    % hold on
    % % plot(p52(:,1), p52(:,2))
    % % plot(p52(:,1), poly_fit(p52(:,1)))
    % plot(p52(:,1), p52(:,2)-poly_fit(p52(:,1)), 'r')
    % hold off
% performing own voight fitting
hold_data = [mhz_248, T_248];
x_min = min(hold_data(:,1));
x_max = max(hold_data(:,1));
x_raw = hold_data(:,1);
x_calc = x_min:1:x_max; %hold_data(:,1);
y_raw = (hold_data(:,2));
    y_raw = y_raw./0.675;
gau_fwhm = 947; %MHz
x_cent = 1082;
ratio = 10; %gaussian to voight
lor_fwhm = 1300:1:1400;
gauss_peak = \exp(-1*(x_calc-x_cent).^2/(2*(gau_fwhm/2.355).^2));
conv_matrix = zeros(length(gauss_peak), length(lor_fwhm));
for k = 1:length(lor_fwhm)
    for m = 1:length(x_calc)
        mul_loop = gauss_peak.*...
        lorenz(x_calc, x_calc(m), 1, lor_fwhm(k));
        conv_matrix(m,k) = trapz(mul_loop);
    end
end
lor_hold = lorenz(x_calc, 1082, 1, 1109);
conv_spline = zeros(length(x_raw), length(lor_fwhm));
residual_mat = zeros(length(x_raw), length(lor_fwhm));
for k = 1:length(lor_fwhm)
    conv_matrix(:,k) = conv_matrix(:,k)./max(conv_matrix(:,k));
    conv_spline(:,k) = spline(x_calc, conv_matrix(:,k), x_raw);
```

```
residual_mat(:,k) = conv_spline(:,k)-y_raw;
    end
    residual_sum = abs(sum(residual_mat(18:41, :), 1));
   % % % testing voight fit using 52 torr data
   \% \text{ cm1}_150 = (\text{mhz}_150./10^3)./29.998;
   \% cent_cm = (cent_1./10^3)./29.998;
   \% \text{ sigma\_cm} = (948/10^3)/29.998;
   \% gamma_cm = (231/10^3)/29.998;
   % par0 = [cent_cm; 0.2; sigma_cm; gamma_cm];
   % dat = [cm1_150, T_150];
   % [parmin,resnom,res,exitflag] = fit2voigt(dat,par0);
   % fit=voigt(cm1_150, parmin);
   %
   % figure
   %
          hold on
   %
          plot(cm1_150, T_150)
   %
          plot(cm1_150, fit)
   %
          hold off
   figure
        hold on
        % plot(p248(:,1), p248(:,2), 'ro')
        % plot(mhz_248, gaus_248(mhz_248)*-1+1, 'r')
        % plot(mhz_150, gaus_150(mhz_150)*-1+1, 'b')
        plot(p150(:,1), p150(:,2), 'bo')
        plot(p52(:,1), p52(:,2), 'mo')
        % plot(mhz_150, gaus_52(mhz_150)*-1+1, 'm')
        hold off
        xlim([-1000 3000])
        xlabel('Relative Optical Frequency (MHz)')
        ylabel('Intensity (a.u.)')
function y = lorenz(x, x_cent, amp, fwhm)
```

end

```
\label{eq:hold_y = (1/pi)*((fwhm/2)./((x-x_cent).^2+(fwhm/2)^2));} y = amp*(hold_y./max(hold_y)); end
```

BIBLIOGRAPHY

- [I] Roberto Barreiro et al. "Experimental demonstration of a new near-infrared spectroscopy technique based on optical dual-comb: DC-NIRS". In: Sci. Rep. 13.1 (2023), p. 10924. DOI: 10.1038/s41598-023-37940-1. URL: https://doi.org/10.1038/s41598-023-37940-1.
- [2] Peter F. Bernath. *Spectra of atoms and molecules*. 2nd ed. Oxford University Press, 2005.
- [3] Robert W. Boyd. *Nonlinear optics*. 2nd ed. Academic Press, 2009, pp. 516–519.
- [4] Brandon Buscaino et al. "Design of Efficient Resonator-Enhanced Electro-Optic Frequency Comb Generators". In: *Journal of Lightwave Technology* 38.6 (2020), pp. 1400–1413. DOI: 10.1109/JLT.2020.2973884.
- [5] David R. Carlson et al. "Ultrafast electro-optic light with subcycle control". In: Science 361.6409 (2018), pp. 1358-1363. DOI: 10.1126/science.aat6451. URL: https://www.science.org/doi/pdf/10.1126/science.aat6451. URL: https://www.science.org/doi/abs/10.1126/science.aat6451.
- [6] Ian Coddington, Nathan Newbury, and William Swann. "Dual-comb spectroscopy". In: Optica 3.4 (2016), pp. 414-426. DOI: 10.1364/OPTICA.3.000414. URL: https://opg.optica.org/optica/abstract.cfm?URI=optica-3-4-414.
- [7] Nicholas D. Cooper, Uyen M. Ta, and Melanie A. R. Reber. "Spectral shaping of an ultrafast ytterbium fiber laser via a passive intracavity optical filter: a simple and reliable route to sub-45fs pulses". In: *Appl. Opt.* 62.9 (Mar. 2023), pp. 2195–2199. DOI: 10.1364/AO.486245. URL: https://opg.optica.org/ao/abstract.cfm?URI=ao-62-9-2195.

- [8] Callum Deakin, Zichuan Zhou, and Zhixin Liu. "Phase noise of electro-optic dual frequency combs". In: *Opt. Lett.* 46.6 (2021), pp. 1345–1348. DOI: 10.1364/OL.418543. URL: https://opg.optica.org/ol/abstract.cfm?URI=ol-46-6-1345.
- [9] I. Debecker, A. K. Mohamed, and D. Romanini. "High-speed cavity ringdown spectroscopy with increased spectral resolution by simultaneous laser and cavity tuning". In: *Opt. Express* 13.8 (2005), pp. 2906–2915. DOI: 10.1364/OPEX.13.002906. URL: https://opg.optica.org/oe/abstract.cfm?URI=oe-13-8-2906.
- [10] S.A. Diddams et al. "Direct RF to optical frequency measurements with a femtosecond laser comb". In: *IEEE Transactions on Instrumentation and Measurement* 50.2 (2001), pp. 552–555. DOI: 10.1109/19.918189.
- [II] Scott A. Diddams et al. "Direct Link between Microwave and Optical Frequencies with a 300 THz Femtosecond Laser Comb". In: *Phys. Rev. Lett.* 84 (22 2000), pp. 5102–5105. DOI: 10.1103/PhysRevLett. 84.5102. URL: https://link.aps.org/doi/10.1103/PhysRevLett.84.5102.
- [12] Jerome M. Dowling. "The rotation-inversion spectrum of ammonia".

 In: J. Mol. Spec. 27.1(1968), pp. 527-538. ISSN: 0022-2852. DOI: https://doi.org/10.1016/0022-2852(68)90058-1. URL: https://www.sciencedirect.com/science/article/pii/0022285268900581.
- [13] Todd Eliason, Payton A. Parker, and Melanie A. R. Reber. "Electro-optic frequency comb generation via cascaded modulators driven at lower frequency harmonics". In: *Opt. Express* 32.21 (Oct. 2024), pp. 36394–36404. DOI: 10.1364/OE.537836. URL: https://opg.optica.org/oe/abstract.cfm?URI=oe-32-21-36394.
- [14] T. Földes et al. "Low-temperature high-resolution absorption spectrum of 14NH3 in the 1+3 band region (1.51 m)". In: *Mol. Phys.* 112.18 (2014), pp. 2407–2418. DOI: 10.1080/00268976.2014.904944. eprint: https://doi.org/10.1080/00268976.2014.904944. URL: https://doi.org/10.1080/00268976.2014.904944.
- [15] Zheng Gong et al. "Monolithic Kerr and electro-optic hybrid microcombs". In: *Optica* 9.9 (2022), pp. 1060–1065. DOI: 10.1364/OPTICA. 462055. URL: https://opg.optica.org/optica/abstract.cfm?URI=optica-9-9-1060.

- [16] E. I. Gordon and J. D. Rigden. "The Fabry-Perot Electrooptic Modulator". In: Bell System Technical Journal 42.1 (1963), pp. 155-179. DOI: https://doi.org/10.1002/j.1538-7305.1963.tb04006.x. eprint: https://onlinelibrary.wiley.com/doi/pdf/10.1002/j.1538-7305.1963.tb04006.x. URL: https://onlinelibrary.wiley.com/doi/abs/10.1002/j.1538-7305.1963.tb04006.x.
- [17] Yang He et al. "High-speed tunable microwave-rate soliton microcomb". In: *Nature Communications* 14.1 (2023), p. 3467. DOI: 10.1038/s41467-023-39229-3. URL: https://doi.org/10.1038/s41467-023-39229-3.
- [18] Nicolas Bourbeau Hébert et al. "Self-heterodyne interference spectroscopy using a comb generated by pseudo-random modulation". In: *Opt. Express* 23.21 (2015), pp. 27806–27818. DOI: 10.1364/OE.23.027806. URL: https://opg.optica.org/oe/abstract.cfm?URI=oe-23-21-27806.
- [19] Nicolas Bourbeau Hébert et al. "Real-Time Dynamic Atomic Spectroscopy Using Electro-Optic Frequency Combs". In: *Phys. Rev. Appl.* 6 (4 2016), p. 044012. DOI: 10.1103/PhysRevApplied.6.044012. URL: https://link.aps.org/doi/10.1103/PhysRevApplied.6.044012.
- [20] James van Howe, Jonas Hansryd, and Chris Xu. "Multiwavelength pulse generator using time-lens compression". In: *Opt. Lett.* 29.13 (2004), pp. 1470–1472. DOI: 10.1364/OL.29.001470. URL: https://opg.optica.org/ol/abstract.cfm?URI=ol-29-13-1470.
- [21] K. Imai et al. "12-THz frequency difference measurements and noise analysis of an optical frequency comb in optical fibers". In: *IEEE Journal of Quantum Electronics* 35.4 (1999), pp. 559–564. DOI: 10.1109/3.753660.
- [22] A. Ishizawa et al. "Ultralow-phase-noise millimetre-wave signal generator assisted with an electro-optics-modulator-based optical frequency comb". In: *Sci. Rep.* 6.1 (2016), p. 24621. DOI: 10.1038/srep24621. URL: https://doi.org/10.1038/srep24621.
- [23] Ken Kashiwagi et al. "Direct generation of 12.5-GHz-spaced optical frequency comb with ultrabroad coverage in near-infrared region by cascaded fiber configuration". In: *Opt. Express* 24.8 (2016), pp. 8120–8131. DOI: 10.1364/OE.24.008120. URL: https://opg.optica.org/oe/abstract.cfm?URI=oe-24-8-8120.

- Yugo Kikkawa et al. "Sub-30-fs fibre-coupled electro-optic modulation comb at 1.5 um with a 25 GHz repetition rate". In: *Electron. Lett.* 59.11 (2023), e12830. DOI: https://doi.org/10.1049/ell2.12830. eprint: https://ietresearch.onlinelibrary.wiley.com/doi/pdf/10.1049/ell2.12830. URL: https://ietresearch.onlinelibrary.wiley.com/doi/abs/10.1049/ell2.12830.
- [25] Tae Shik Kim and Benjamin J. Vakoc. "Stepped frequency comb generation based on electro-optic phase-code mode-locking for moderate-speed circular-ranging OCT". In: *Biomed. Opt. Express* 11.7 (2020), pp. 3534–3542. DOI: 10.1364/BOE.392359. URL: https://opg.optica.org/boe/abstract.cfm?URI=boe-11-7-3534.
- [26] Abijith S. Kowligy et al. "Mid-infrared frequency combs at IoGHz". In: Opt. Lett. 45.13 (2020), pp. 3677-3680. DOI: 10.1364/OL.391651. URL: https://opg.optica.org/ol/abstract.cfm?URI=ol-45-13-3677.
- Nicholas J. Lambert, Luke S. Trainor, and Harald G. L. Schwefel. "Microresonator-based electro-optic dual frequency comb". In: *Communications Physics*6.1 (2023), p. 89. DOI: 10.1038/s42005-023-01197-x. URL: https://doi.org/10.1038/s42005-023-01197-x.
- [28] Can Li et al. "Hybrid WDM-MDM transmitter with an integrated Si modulator array and a micro-resonator comb source". In: *Opt. Express* 29.24 (2021), pp. 39847–39858. DOI: 10.1364/0E.444493. URL: https://opg.optica.org/oe/abstract.cfm?URI=oe-29-24-39847.
- [29] Jiang Li et al. "Electro-optical frequency division and stable microwave synthesis". In: Science 345.6194 (2014), pp. 309-313. DOI: 10.1126/science.1252909. eprint: https://www.science.org/doi/pdf/10.1126/science.1252909. URL: https://www.science.org/doi/abs/10.1126/science.1252909.
- [30] D. A. Long et al. "Multiplexed sub-Doppler spectroscopy with an optical frequency comb". In: *Phys. Rev. A* 94 (6 2016), p. 061801. DOI: 10.1103/PhysRevA.94.061801. URL: https://link.aps.org/doi/10.1103/PhysRevA.94.061801.
- [31] D. A. Long et al. "Single-modulator, direct frequency comb spectroscopy via serrodyne modulation". In: *Opt. Lett.* 48.4 (2023), pp. 892–895. DOI: 10.1364/OL.482597. URL: https://opg.optica.org/ol/abstract.cfm?URI=ol-48-4-892.

- [32] Isao Morohashi et al. "Widely repetition-tunable 200 fs pulse source using a Mach–Zehnder-modulator-based flat comb generator and dispersion-flattened dispersion-decreasing fiber". In: *Opt. Lett.* 33.II (2008), pp. II92–II94. DOI: 10.1364/OL.33.001192. URL: https://opg.optica.org/ol/abstract.cfm?URI=ol-33-11-1192.
- [33] H. Murata et al. "Optical pulse generation by electrooptic-modulation method and its application to integrated ultrashort pulse generators". In: *IEEE Journal of Selected Topics in Quantum Electronics* 6.6 (2000), pp. 1325–1331. DOI: 10.1109/2944.902186.
- [34] S. Nouri et al. "Temperature dependence of pressure broadening of NH3 perturbed by H2 and N2". In: J. Mol. Spec. 227.1 (2004), pp. 60-66. ISSN: 0022-2852. DOI: https://doi.org/10.1016/j.jms.2004.05.009. URL: https://www.sciencedirect.com/science/article/pii/S0022285204001560.
- [35] Nathalie Picqué and Theodor W. Hänsch. "Frequency Comb Spectroscopy". In: *Nat. Photonics* 13.3 (2019), pp. 146–157. DOI: 10.1038/s41566-018-0347-5. URL: https://doi.org/10.1038/s41566-018-0347-5.
- [36] Shunda Qiao, Ying He, and Yufei Ma. "Trace gas sensing based on single-quartz-enhanced photoacoustic-photothermal dual spectroscopy". In: Opt. Lett. 46.10 (2021), pp. 2449-2452. DOI: 10.1364/OL.423801. URL: https://opg.optica.org/ol/abstract.cfm?URI=ol-46-10-2449.
- [37] T. Saitoh, M. Kourogi, and M. Ohtsu. "Expansion of span-width of an optical frequency comb using a higher harmonic wave modulation". In: *IEEE Photonics Technology Letters* 8.10 (1996), pp. 1379–1381. DOI: 10.1109/68.536661.
- [38] Minhyup Song et al. "Programmable and tunable flat-top supercontinuum laser sources via electro-optic intensity and phase modulation scheme". In: *Sci. Rep.* 12.1 (2022), p. 18036. DOI: 10.1038/s41598-022-22463-y. URL: https://doi.org/10.1038/s41598-022-22463-y.
- [39] G.-W. Truong et al. "Frequency-Agile, Rapid Scanning Spectroscopy". In: *Nat. Photonics* 7.7 (2013), pp. 532-534. DOI: 10.1038/nphoton. 2013.98. URL: https://doi.org/10.1038/nphoton.2013.98.

- [40] C. H. Valahu et al. "Direct observation of geometric-phase interference in dynamics around a conical intersection". In: *Nat. Chem.* 15.11 (2023), pp. 1503–1508. DOI: 10.1038/s41557-023-01300-3.
- [41] Nathanial Wilson et al. "Simultaneous Observation of Nonlinear Magneto-Optical Rotation in the Temporal and Spectral Domains with an Electro-Optic Frequency Comb". In: *Phys. Rev. Appl.* 10 (3 2018), p. 034012. DOI: 10.1103/PhysRevApplied.10.034012. URL: https://link.aps.org/doi/10.1103/PhysRevApplied.10.034012.
- [42] Ji-Liang Wu et al. "Optical frequency comb and picosecond pulse generation based on a directly modulated microcavity laser". In: *Appl. Opt.* 60.14 (2021), pp. 4177–4184. DOI: 10.1364/AO.423912. URL: https://opg.optica.org/ao/abstract.cfm?URI=ao-60-14-4177.
- [43] Shijun Xiao et al. "Toward a low-jitter 10 GHz pulsed source with an optical frequency comb generator". In: *Opt. Express* 16.12 (2008), pp. 8498–8508. DOI: 10.1364/OE.16.008498. URL: https://opg.optica.org/oe/abstract.cfm?URI=oe-16-12-8498.
- [44] Bingxin Xu et al. "Wideband and high-resolution spectroscopy based on an ultra-fine electro-optic frequency comb with seed lightwave selection via injection locking". In: *Opt. Lett.* 46.8 (2021), pp. 1876–1879. DOI: 10.1364/OL.420377. URL: https://opg.optica.org/ol/abstract.cfm?URI=ol-46-8-1876.
- [45] Ruitao Yang et al. "Analysis of a highly efficient phase-locking stabilization method for electro-optic comb generation". In: *Appl. Opt.* 59.16 (2020), pp. 4839–4848. DOI: 10.1364/A0.389138. URL: https://opg.optica.org/ao/abstract.cfm?URI=ao-59-16-4839.
- [46] Amnon Yariv. "Phase Modulation of Light". In: *Optical Electronics*. 3rd ed. CBS College publishing, 1985, pp. 294–296.
- [47] Jun Ye and Steven T. Cundiff. Femtosecond Optical Frequency Comb: Prinfiple, Operation and Applications. Springer New York, NY, 2005.
- [48] Ke Zhang et al. "A power-efficient integrated lithium niobate electro-optic comb generator". In: *Commun. phys.* 6.1 (2023), p. 17. DOI: 10. 1038/s42005-023-01137-9. URL: https://doi.org/10.1038/s42005-023-01137-9.
- [49] Xin Zhang et al. "Optical frequency comb assisted reconfigurable broadband spread spectrum signal generation". In: *Opt. Express* 31.26 (2023), pp. 42866–42877. DOI: 10.1364/OE.506620. URL: https://opg.optica.org/oe/abstract.cfm?URI=oe-31-26-42866.

[50] Rongjin Zhuang et al. "Electro-Optic Frequency Combs: Theory, Characteristics, and Applications". In: Laser Photonics Rev. 17.6 (2023), p. 2200353. DOI: https://doi.org/10.1002/lpor.202200353. eprint: https://onlinelibrary.wiley.com/doi/pdf/10.1002/lpor.202200353. URL: https://onlinelibrary.wiley.com/doi/abs/10.1002/lpor.202200353.